New Insights into Interpretation of Aeromagnetic Data for Distribution of Igneous Rocks in Central Iran

Мохаммадзадех Могхаддам М. ., Мирзаеи С. ., Абеди М. .

Аннотация

New insights in the aeromagnetic data over the Central Iranian Microcontinent (CIM) revealed interesting results for future studies and exploration. This work presents the interpretation of different magnetic analysis and calculated 3D inversion models in order to realize igneous rock distribution within regions that could be traced under significant cover. The analysis of a significant amount of data on magnetic susceptibility and igneous rock aeromagnetic anomalies in the area indicated that mafic-ultramafic intrusive rocks contain a significant degree of magnetic susceptibility in general and generate considerable magnetic responses. Intermediate-felsic intrusive rocks are slightly magnetically susceptible and exhibit a smooth gradient change and a typically regular shape. There is a wide range of susceptibility in volcanic rocks. As a result, aeromagnetic anomalies most commonly occur randomly or exhibit strong amplitude with high-frequency signals which are quickly eliminated by the application of upward continuation. According to the analysis of different magnetic maps and 3D data inversion and the combination of such information with known igneous rocks outcropped, we revealed 1215 concealed intrusive rocks and 528 volcanic rocks in the area. In addition, the boundaries of many outcropped igneous rocks were reproduced. It is possible to classify the well-known and newly-mapped igneous rocks into twelve regions (or zones) for intrusive rocks and four regions for volcanic rocks. It was observed that a majority of mafic-ultramafic rocks lie in Sistan Suture Zone in eastern Iran along Nehbandan Fault Zone. It was also found that many parts of Lut Block, as a basic portion of CIM, have been under magmatic events; thus, most of the concealed igneous rocks are distributed in the middle and southern parts of Lut Block. Volcanic rocks are widely developed in the southeastern and northern parts of the area, such as Urumieh-Dokhtar Magmatic Arc, North Lut, and Bam region.

Ключевые слова:

Aeromagnetic data, Central Iran, Magnetic susceptibility, 3D inversion, Concealed igneous rocks

New insights into interpretation of aeromagnetic data for distribution of igneous rocks in Central Iran

Mohammad Mohammadzadeh Moghaddam[1]*, Saeed Mirzaei[1] and Maysam Abedi[2]

[1]Research Institute of Applied Sciences, Shahid Beheshti University, Tehran, Iran
[2]School of Mining Engineering, College of Engineering, University of Tehran, Iran

Abstract

New insights in the aeromagnetic data over the Central Iranian Microcontinent (CIM) revealed interesting results for the future studies and exploration. This work presents the interpretation of the different magnetic analysis and calculated 3D inversion model to provide important insights into the distribution of igneous rocks in the area that may be traced under significant cover. By analyzing several hundred magnetic susceptibility data points and aeromagnetic anomalies of known igneous rocks over the area, it was determined that mafic-ultramafic intrusive rocks generally have a high magnetic susceptibility and produce strong magnetic response. Intermediate-felsic intrusive rocks have a low magnetic susceptibility and show a smooth gradient variation and commonly regular shape. Volcanic rocks show a wide range of magnetic susceptibility; therefore, the aeromagnetic anomalies are often random or show strong amplitude with high frequency signals which is eliminated rapidly when an upward continuation is applied. Based on results of analysis of different magnetic map and 3D inversion of data, and combining this information with known outcropped of igneous rocks, we revealed 1215 concealed intrusive rocks and 528 volcanic rocks in the area. We also renewed the boundaries of tens outcropped igneous rocks. The known and new mapped igneous rocks can be identified as 12 regions (or zones) for intrusive rocks and 4 regions for volcanic rocks. The results indicate that the mafic-ultramafic rocks are mainly located in Sistan suture zone of eastern Iran along Nehbandan fault zone. It also shows that the many parts of Lut block as a main portion of CIM has been under magmatic events, so that the most of concealed igneous rocks is distributed in the middle and southern part of Lut block. Volcanic rocks are widely developed in southeastern and northern parts of the area such as Urumieh-Dokhtar Magmatic Arc, North Lut and Bam region.

Keywords: Aeromagnetic data, Central Iran, Magnetic susceptibility, 3D inversion, Concealed igneous rocks

1. Introduction

Resolution of the magmatic history of Central Iran has been hampered by a lack of high-resolution geophysical data for the accurate delineation of igneous rocks under significant cover. Recently the Geological Survey of Iran (GSI) has been reprocessed historical semi-high resolution aeromagnetic data over the area for a better understanding of the subsurface structures. The investigation of igneous rocks is important to developing a mean for studying tectonic evolution and mineral exploration. The area extends from south of Birjand in the north, to Bazman in the south, through Nehbandan and Nayband, and include a significant portion of Central Iranian Microcontinent (CIM), Urumieh-Dokhtar Magmatic Arc (UDMA) and Sanandaj-Sirjan Zone (SSZ) in the southwest (Fig. 1).

Traditional methods such as field observations and newer methods such as analysis of satellite images are the main ways for mapping igneous rocks. These methods are usually useful for outcropped units, whereas the other igneous rocks which are concealed by overburden covers or are exposed only in highly inaccessible areas, escape detection. Therefore, airborne magnetic method is the most effective tool for better identification of known igneous rocks and detection of concealed ones (Xiong et al., 2016).

Aeromagnetic anomalies are usually caused by magnetic contain of the underlying rocks' magnetic properties which is known as magnetic susceptibility. In general, sedimentary and metamorphic rocks have the lower magnetic susceptibility rather igneous rocks. Mafic minerals such as magnetite have most magnetic susceptibility. Therefore, with increase of mafic minerals, the magnetic field intensity of the rocks becomes stronger (Gunn, 1997). By interpretation of aeromagnetic data over an area especially over a sedimentary basin, it would be possible to map magnetic basement (igneous and/or metamorphic) rocks and concealed igneous bodies such as intrusive dykes, sills and volcanic rocks (e.g. Abdelsalam et al., 2016; Anudu et al., 2014; Behrendt, 2013; Chernicoff et al., 2012; Finn and Morgan, 2002; Galindo-Zaldívar et al., 2013; Mietha et al., 2014; Xiong et al., 2016). These igneous units may play an important role as heat sources of a geothermal system such as Mahallat geothermal system (Mohammadzadeh et al., 2015; Oskooi et al., 2016), responsible for polymetallic and porphyry copper deposits (Kheyrollahi et al., 2018) or a hydrocarbon system (Xu et al., 2009) in Iran.

This new interpretation of aeromagnetic data over the CIM provides unprecedented resolution of deep magmatic activities that is pivotal to understanding the geological history of Iran and the assembly of adjacent Tethyan or Cimmerian areas (Barrier and Vrielynck, 2008). The interpretation was integrated, in a separate study, with an extensive suite of other data, including mineral deposits and occurrences in order to develop a model-driven, mineralization systems approach and to prioritize areas for different types of mineralization.

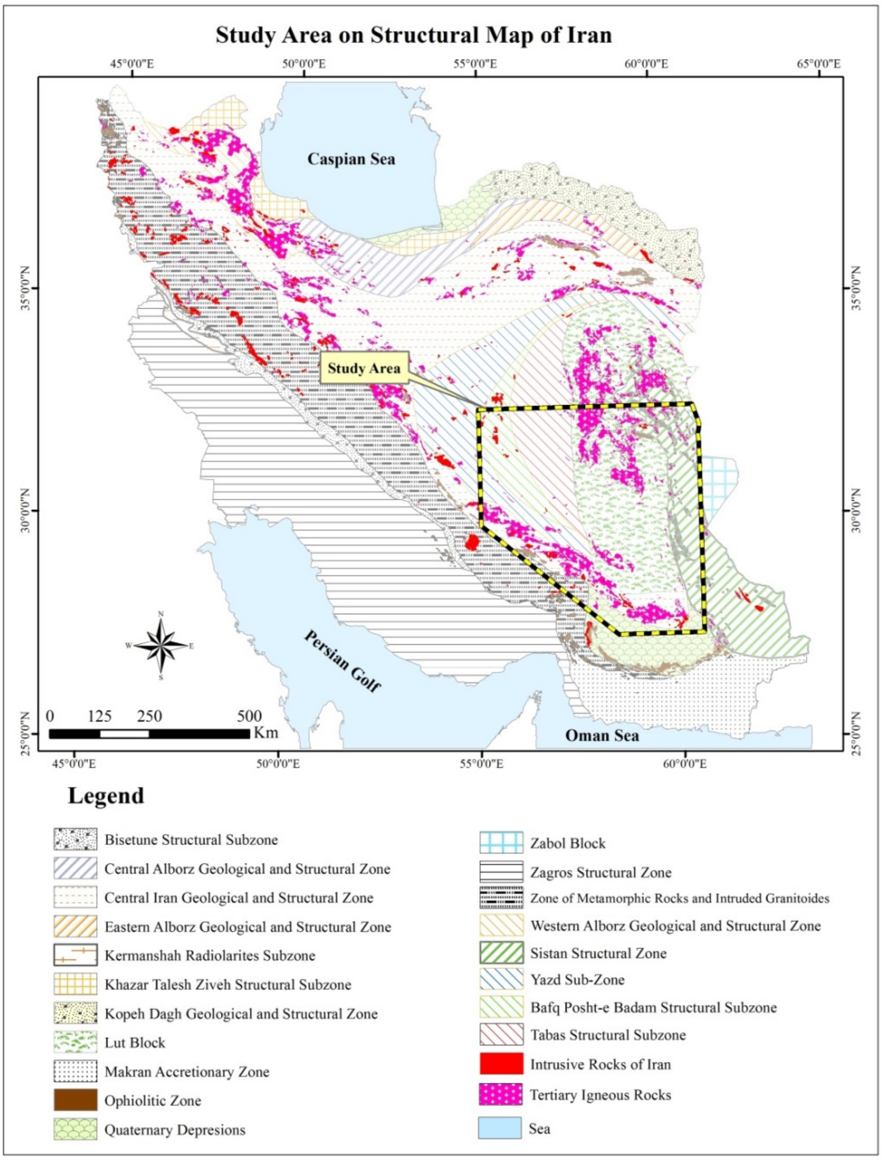

Fig. 1. Study area on structural map of Iran (Nogol-Sadat, 1993).

2. Geological history

The Central Iranian Microcontinent (CIM) is situated in the Alpine-Himalayan orogenic system and is portion of the large Cimmerian continent, which evolved during the closure of the Paleotethys Ocean (e.g. Stöcklin, 1968; Sengör, 1987).

Iran and the surrounding areas are from continental blocks in the Alpine-Himalayan orogenic belt, which were distinct by complex fold and thrust belts (Gansser et al., 1981). Indeed, Iran and the adjacent continents are a composite crust of the continental blocks detached from Gondwana supercontinent and continuously attached to the southern Eurasia after passing through Tethys Ocean. At commence of the Early Permian, a long narrow piece of continental blocks, made up of parts of Turkey and Iran (Cimmerian blocks), detached from northern Gondwana (Brunet et al., 2009). Cimmerian continental blocks rapidly drifted northward across of Paleotethys during Early Permian to Late Early Triassic (Muttoni et al., 2009). The collision of Cimmerian blocks including Iran against southern Asia resulted in the Eo-Cimmerian orogeny (Stille, 1910), which led to the closure of the Paleozoic Paleotethys ocean (Berberian and King, 1981; Sengör, 1990; Stampfli and Borel, 2002).

3. Data sets

Airborne magnetic data acquisition is a rapid, cost effective means of identifying geological units under cover. From 1976 to 1978, semi-detailed airborne magnetic data were collected at a 1000 m and 2000 m line spacing in several flight blocks. A 041° traverse orientation, with 1:10 traverse-to-tie line spacing ratio, was employed throughout of the survey. Nominal survey heights of 120 m were used and data were collected using a caesium-vapour magnetometer with 0.01 gamma recording sensitivity. After data correction and processing, the blocks were merged with a robust leveling and micro-leveling over the data of study area. Data were gridded on a 1:5 cell size vs. line spacing ratio. The IGRF model 1975 was utilized to remove the variation of the core field of the earth to prepare the residual Total Magnetic Intensity (TMI) map. Filters and products of this data, which form the basis of the interpretation, are Total Magnetic Intensity (TMI), reduction to pole (RTP), First and Second Vertical Derivative (VD1, VD2), Tilt Derivative (TDR), Regional and Residual (using spectral analysis) and upward continuation. Fig. 2 show reduced to pole (RTP) map of the area which calculated by differential reduction-to-the-pole method (Arkani-Hamed, 2007). Unlike the traditional RTP algorithms, Baranov (1957) and Fedi et al. (1994) methods, which use a fixed inclination and declination for all data, the algorithm proposed by Arkani-Hamed (2007) utilizes the inclination and declination of each data instance separately for the application of the RTP filter.

The interested area is located within several regional, historical data sets, which are described in Table 1. These comprise regional magnetic data with 7.5 km line spacing from 1970s; the interpretational contour map of the regional aeromagnetic survey, Bouguer gravity data of BGI based regional ground gravimetric survey from 1970s, satellite images and geological data. SRTM data were obtained from NASA shuttle missions, during which a single-pass interferometric radar system was deployed (Farr et al., 2007). Data are available for download as degree tiles at http://srtm.csi. cgiar.org/SELECTION/inputCoord.asp (Jarvis et al., 2008), and comprise 90m spatial resolution DEMs (Digital Elevation Models). To enhancement of different structural trends, a mosaic of SRTM tiles was generated for Iran, whilst shaded relief images, with various sun azimuths.

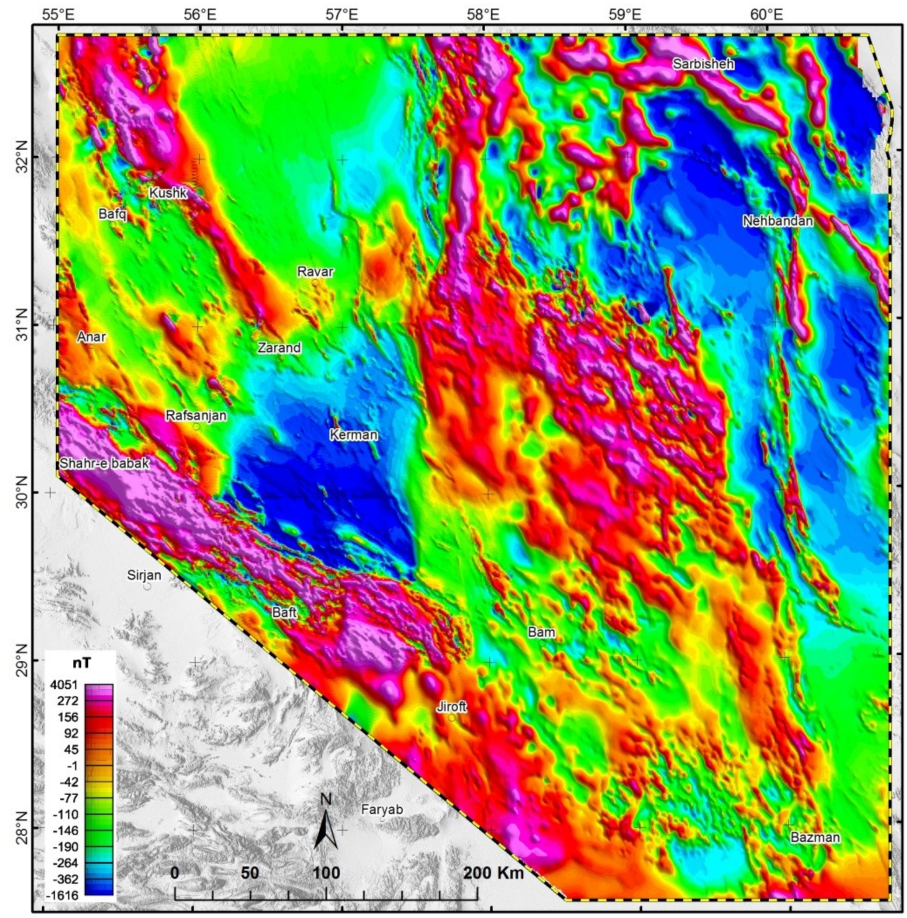

Fig. 2. Aeromagnetic image (TMI) of Central Iran.

Table 1. Summary of regional data set.

Dataset	Data type	Data format	Actions
Geophysical	National Regional Aeromagnetic Data	Geosoft grids	Stitched individual grids and re-gridded to provide a continuous integrated grid
	1:250 000 interpretation of magnetic data contour sheets	Georeferenced images	None
	Ground-based gravity data processed by BGI	Geosoft grid	None
Geological	1:1000 000 Tectonic map of Iran	jpg image	Georeferenced. Mosaic and spatial join to form an integrated coverage
	1:1000 000 Magmatic map of Iran (Emami et al., 1993)	jpg image	Georeferenced. Mosaic and spatial join to form an integrated

			coverage
	1:250 000 Geology map sheets	jpg image	Georeferenced. Mosaic and spatial join to form an integrated coverage
	1:100 000 Geology map sheets	jpg image	Georeferenced. Mosaic and spatial join to form an integrated coverage
	1:250 000 Vector geology	Shapefile	Recoded data fields according to 1:250 000 map sheets
Satellite	Landsat (full individual scenes)	FST and geotiff	
	MrSID image	.sid (raster file)	
	SRTM 90m DEM's	ArcGIS format	Generated sun-shaded relief images

4. Analysis and interpretation

4.1. Magnetic susceptibility of igneous rocks

The magnetic intensity of materials in an external magnetic field is controlled by the proportionality coefficient K, known as magnetic susceptibility. When a substance is placed in the magnetic field H, the magnetism induced in the substance M is defined as $K=M/H$. Recognition of the physical properties of rocks in an area (such as magnetic susceptibility, density, etc.) is critical in determining the geophysical method and data interpretation (Clark et al., 1997). Interpretation of aeromagnetic data must be performing with enough knowledge of magnetic susceptibility of the rocks in study area. To map igneous rock units using aeromagnetic data, we first integrated and analyzed hundreds of magnetic susceptibility data points that have been measured from different types of outcropped igneous units in Central Iran and surrounding areas. These data have been measured mainly during the last decade in various exploration projects, especially iron exploration projects by mining companies and organizations in Iran (e.g. Sadeghian and Valizadeh, 2008; Alamdar, et al., 2012). Most of these data has not been made public and has only been archived by internal reports of Iranian companies and organizations.

After the initial processing, we classified all magnetic susceptibility data into three rock types: mafic-ultramafic, intermediate-felsic, and volcanic (Table 2). The results show distinct magnetic susceptibilities of different types of igneous rocks. Generally mafic-ultramafic rocks have high magnetic susceptibility and ranging from 0.02 to 0.6 SI. The average value of these types of igneous rocks is 0.05 SI. Statistical averages show that after magnetite, ultramafic rock units (such as pyroxenite and peridotite) have the highest magnetic susceptibility, whereas magnetic susceptibility of mafic rock units (such as diabase) is lower. Magnetic susceptibility of intermediate-felsic rocks is usually lower than mafic-ultramafic rocks. The Magnetic susceptibility values of this group range from zero to 0.1 SI with an average of 0.014 SI. The third rock type is volcanic rocks that show a wide range of magnetic susceptibility. The results show the magnetic properties of volcanic rocks are sharply changed, but the magnetic susceptibilities values are low with an average of 0.19 SI.

Table 2. Statistics of the magnetic susceptibility of different types of igneous rocks in Central Iran.

Rock type	Lithology	Magnetic susceptibility (K, 10^{-3} SI)		Mean of each type
		Range	Mean	
Mafic-ultramafic rock	Ultramafic rocks	25-172	54	48
	Magnetite	42-550	189	
	Peridotite	20-146	76	
	Pyroxenite	20-115	83	
	Gabbro	20-105	37	
	Diabase	30-98	24	
Intermediate-felsic rock	Diorite	7-97	19	14
	Syenite	5-79	41	
	Granite	0-44	5	
	Granodiorite	0-51	6	
Volcanic rock	Basalt	12-178	28	19
	Trachyte	10-270	9	
	Andesite	10-188	21	
	Rhyolite	0-68	12	
	Tuff	0-130	16	

3.2. Analysis of VD1 and AS data

After analyzing magnetic susceptibility of different types of igneous rocks, aeromagnetic anomalies have been analyzed to determine the significant features of the aeromagnetic anomalies for each type of igneous rocks including anomaly shape, size, intensity, and frequency. Because the aeromagnetic anomalies caused by igneous rocks are usually mixed with the background fields and cannot be distinguished easily, so the processing methods such as vertical derivative and analytical signal are needed to utilize over the original aeromagnetic data, to separate different anomalies of the igneous bodies and define their boundaries (Xiong et al., 2016). The vertical first order derivative (VD1) and analytical signal (AS) methods are very effective in estimating the domain and boundaries of shallow magnetic bodies. In practice, we can consider the value more than zero of first order vertical derivative map as the boundaries of the magnetic bodies (Fig. 3). The analytical signal method is also effective tool to estimate the boundaries of shallow magnetic fields. With different cutoff of the analytical data of Central Iran's aeromagnetic data, we concluded the values more than 0.05nT/m have a good correlation with the shallow magnetic bodies in the area (Fig. 4). It should be noted that the identification of concealed bodies in the study area requires an integrated study of geological and geophysical information; therefore, magnetic maps are used as an information layer to detection of concealed igneous bodies.

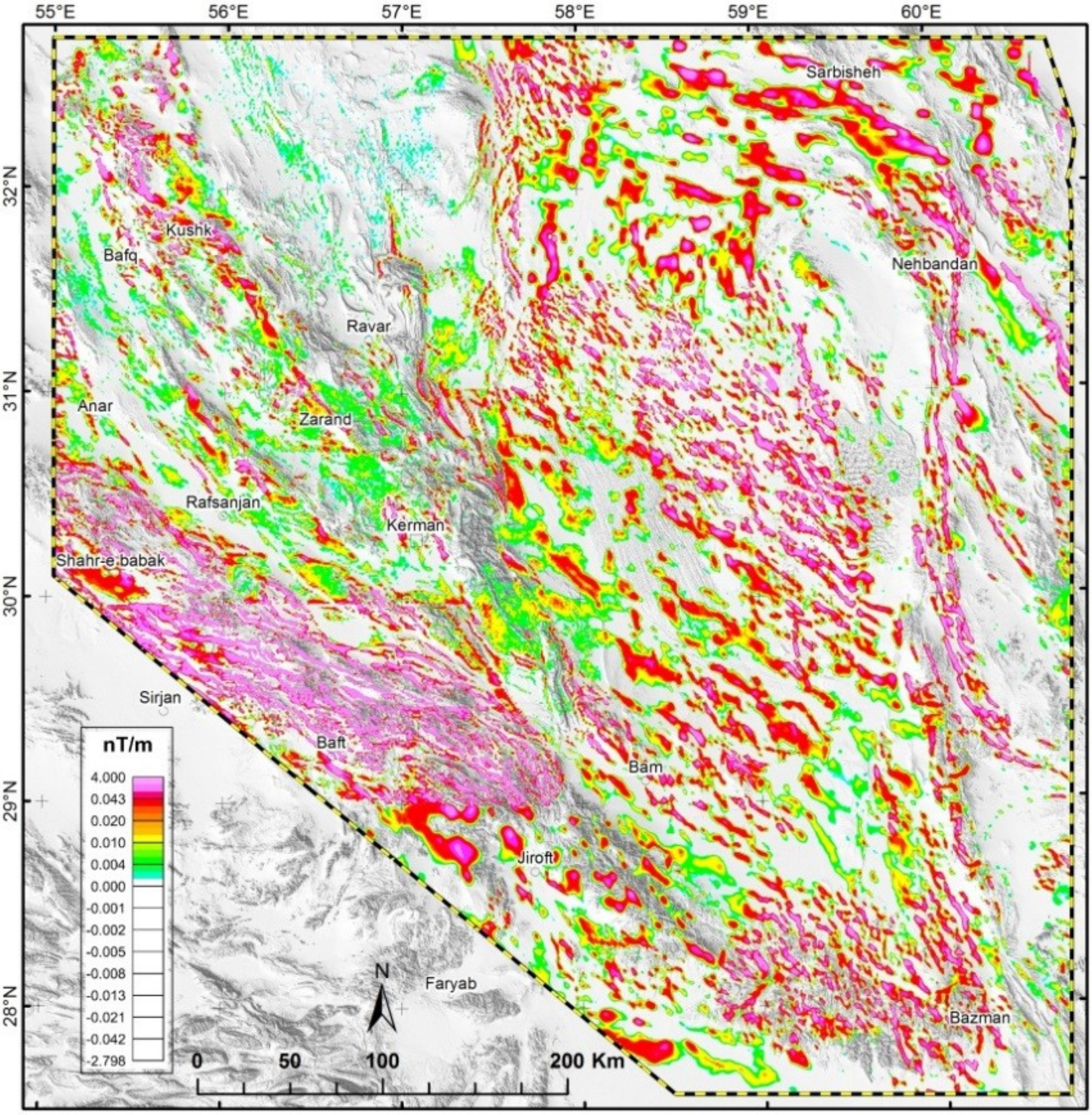

Fig. 3. The values more than zero of the vertical first order derivative data

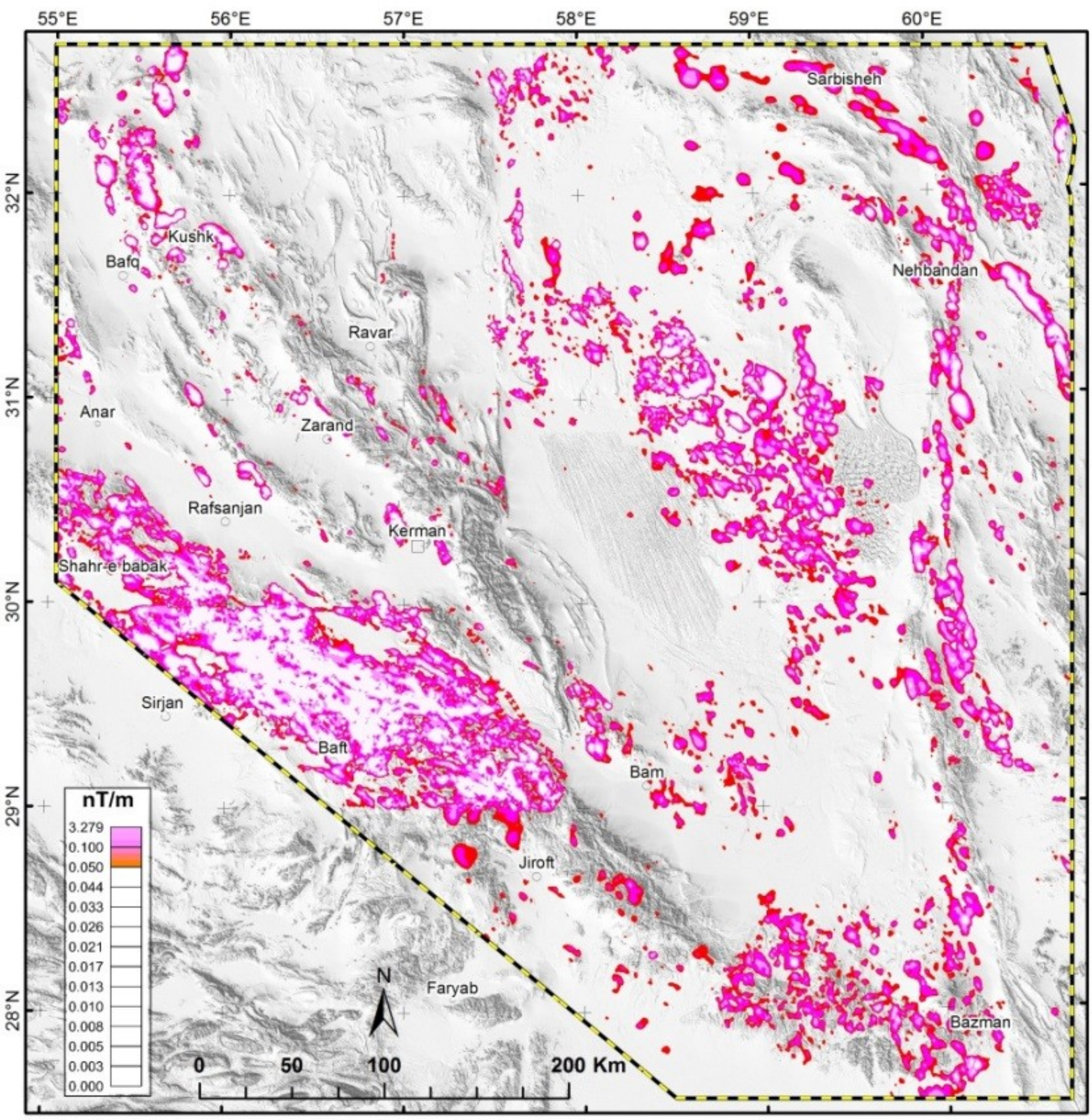

Fig. 4. The values more than 0.05nT/m of the analytical signal data

3.3. Aeromagnetic anomalies of igneous rocks

Igneous rocks are classified two types: intrusive (plutonic) and extrusive (volcanic) rocks. These two types of igneous rocks differ in terms of formation, chemical composition and percentage of magnetic substances. In this section we are analyzed the magnetic response of these rocks.

3.3.1. Intrusive rocks

Aeromagnetic anomalies produced by intrusive rocks usually feature an isometric, ellipse or belt shape (Xiong et al., 2016). With the presence of mafic minerals the magnetic susceptibility of igneous rocks increases gradually from felsic to ultramafic (Table 2). The magnetic response could be different despite the same type of intrusions, because of different geological settings and different time of rock formation. Meanwhile, the buried depth and the volume of the intrusive rocks is also affected the amplitude of the magnetic anomalies. Different chemical compositions of intrusive bodies directly effect on the amplitude of the magnetic signal, therefore mafic and ultramafic bodies create a strong magnetic anomaly, whereas intermediate and felsic bodies create a weaker magnetic anomaly. Following we are analyzed the magnetic anomalies of different intrusive rocks.

(1) Mafic-ultramafic rocks

Mafic-ultramafic intrusive bodies of rocks are generally ophiolite complexes. These rocks commonly show a high magnetic susceptibility ranging from 0.02 to 0.6 SI. For example, the magnetic susceptibility of peridotite ranges from 0.02 to 0.15 SI with an average of 0.08 SI, whereas the average value of gabbro is 0.04 SI. Whether the rock is mafic or ultramafic, the existences of similar magnetic properties make it difficult to identify from the aeromagnetic data. Therefore, in this study, the strong magnetic anomalies present an aeromagnetic anomaly zone or linear anomaly belt with high intensity along a deep fault zone are caused by mafic-ultramafic rocks. The magnetic intensity of these rock units is usually strong and shows an abrupt increase in aeromagnetic anomaly to $n \times 100$ or even sometimes to 1000 nT.

(2) Intermediate-felsic rocks

Intermediate-felsic rocks are mainly including diorite (quartz diorite and diorite porphyrite) and granitoids (granodiorite, granite, granite porphyry, biotite granite and leucogranite). These rocks are distributed in different geological background and produce magnetic anomalies with a different shapes and intensities. According susceptibility data, the magnetic response of the intermediate-felsic rocks is obviously weaker than the mafic-ultramafic rocks. The magnetic susceptibility mainly ranges from zero to 0.02 SI and rarely reaches 0.1 SI. Moreover, the values of intermediate rocks (average for diorite = 0.02 SI, syenite = 0.04 SI) are higher than the felsic rocks (average for granite = 0.005 SI and leucogranite close to zero). The same type of rocks with the same lithology may present distinct magnetic susceptibilities, due to the different geological time and background. By analyzing the aeromagnetic anomalies of known rocks, revealed the magnetic intensity generally decreases from diorite to granodiorite to granite. Both diorite and granodiorite can produce significant magnetic anomalies; however such anomalies are unclear when the rock volume is smaller. In the aeromagnetic map, most of the granites can be identified and feature broad magnetic variation and some of them may be nonmagnetic (such as Zarrin Granite and Tut Granite in northwest of the area) and show a negative anomaly on the aeromagnetic map. However, due

to the enrichment of magnetic minerals by thermal metamorphism in the host rock, there is usually a circular anomaly around these non-magnetic granitic massifs. This feature can be used to outline the intermediate-felsic rocks with weak or non-magnetic anomalies (Zhu, 2013). Magnetic anomalies produced by intermediate and felsic rocks ranges from n × 10 to n × 100 nT with a flat gradient and regular shape, either as an ellipse region or a linear belt.
To map the intrusive rocks, it is necessary to eliminate the anomalies produced by volcanic, metamorphic and other magnetic rocks and combine them with geological and geophysical data. The boundary of the intrusive rocks can be concluded in one of following ways:

- take the gradient zone as the boundary of the rocks on the RTP map;
- take the zones with more than zero values on the map of the vertical first order derivative when the aeromagnetic anomaly is smaller or unclear;
- take the inner zone of circle anomalies produced by ring structure;
- take the zone with above the 0.05 nT/m on the analytic signal map.

3.3.2. Volcanic rocks

Volcanic rocks, such as basalt, andesite, tuff, lava, volcanic breccia, rhyolite and trachyte, are magnetically heterogeneous with a significant magnetic remanence because of the rapid solidification during the eruption of magma to the surface. The volcanic rocks' susceptibility is changed over a wide range (Table 2). The average susceptibility values of volcanic rocks are lower than mafic-ultramafic rocks. The susceptibility data slightly decreases from mafic to felsic volcanic rocks; for instance the average values of basalt, andesite and rhyolite are 0.028, 0.021 and 0.012 SI, respectively.
The anomalies produced by these rocks are featured by an abrupt variation along the survey profile with a strong amplitude and higher gradient, and by a ring, semi-ring or irregular belt with a planar sprawling variation on the RTP map. The basalts have intense magnetic anomaly with a wide range of variation from n × 10 to n × 100 or n × 1000 nT, whereas andesite is lower than basalt and ranges from n × 10 to n × 100 nT. These anomalies sharply changed in the RTP map and decrease quickly when an upward continuation is applied.

3.4. Three-dimensional inversion

Three-dimensional susceptibility contrast model was calculated with the UBC-GIF Mag3D software with the algorithms of Li and Oldenburg (1996), which has been used often with interesting results (e.g. Oldenburg and Pratt, 2007; Louro and Mantovani, 2013; Mohammadzadeh et al, 2015). This algorithm starts from the Eq. 1:

$$d = Gk$$

(1)

Where d is the vector of real which is extracted in the survey, G is sensitivity matrix and m is the susceptibility vectors of the tri-orthogonal mesh to be created for the inversion.

The inverse problem can be formulated as an optimization problem where an objective function of the model is minimized subject to the constraints in Eq.1. The objective function of the density model in Eq. 2 is minimized under determined constraints in order to reproduce data inside an error tolerance.

$$\varnothing_m(m) = \alpha_s \int_v w_s \{ w(r) [m(r) - m_0] \}^2 dv$$

$$+ \alpha_x \int_v w_x \left\{ \left[\frac{\partial w(r)}{\partial x} \right] (m(r) - m_0) \right\}^2 dv$$

$$+ \alpha_y \int_v w_x \left\{ \left[\frac{\partial w(r)}{\partial y} \right] (m(r) - m_0) \right\}^2 dv$$

$$+ \alpha_z \int_v w_z \left\{ \left[\frac{\partial w(r)}{\partial z} \right] (m(r) - m_0) \right\}^2 dv \qquad (2)$$

where m is the magnetic model element, m_0 reference model, w_s , w_x , w_y, and w_z weighting functions, α_s , α_x , α_y and α_z coefficients which affect relative importance of different components in objective function and $w(r)$ the generalized depth weighting function. This function has flexibility to construct many various models. The aim of the objective function is to counteract geometrical decay of the sensitivity with the distance from observation location so that the recovered magnetic susceptibility is not concentrated near observation locations. In the next step, data misfit is calculated ($\varnothing_d$) between observed data and predicted data using Eq. 3:

$$Gk - ¿$$
$$w_d (¿ d_{obs}) ||$$
$$¿$$
$$¿$$
$$\varnothing_d = ¿ \qquad (3)$$

w_d is a diagonal matrix in which the ith element is standard deviation of the ith datum, G is the sensitivity matrix, k the predicted susceptibility vector and d_{obs} is observed data. The inversion objective is minimizing of differences between both objective function and data misfit:

$$\varnothing = \varnothing_d + \mu \varnothing_m \quad (4)$$

In which μ is a regularization parameter that controls relative importance of the model norm and data misfit.

The described methodology provides a basic structure for solving 3D magnetic inversion. More solutions of Mag3D are available in Li and Oldenburg (1996).

In this method, the speed of implementation of inversion is depended mainly on the number of input data and the number of cells (mesh). With choosing of a greater number of input data and smaller size of meshes, the inversion time will be increased. Because our study area is very large, we decided to divide the whole area into 23 separated blocks with dimensions of 120 × 120 km to overcome the limitations of the algorithm on the number of input data points and the number of cell size (Fig. 5). As shown in this figure, a 10 km overlap is considered for adjacent blocks to remove edge effects of the inversion. Each block was inverted separately and thus 23 recovered models were obtained from the area. In order to create a combined model, all the inverted data were merged and integrated. In this inversion, with considering the scale of area and expected resolution, the dimension of each mesh were determined with 800 × 800 × 400 m. The inversion process was performed by a computer with Core i5, CPU 2.5 GHz, RAM 6GB, and Cash 6M specifications. The inversion time took about 7 to 12 hours for each block and a total of about 10 continuous days took the inversion for the whole area.

After merging the inversion data, an integrated model was obtained for the area (Fig. 6a). This model shows the magnetic susceptibility of rocks and materials from the surface to a depth of 6 km. As shown in Fig.6, the maximum recovered magnetic susceptibility is about 0.2 SI. Using this model, it is possible to analyze all zones related to shallow and deep bodies. Due to the importance of magnetic susceptibility of rocks in detecting different types of igneous rocks in Central Iran, the recovered model was classified in five groups in terms of calculated magnetic susceptibility as Fig. 6b to 6f. These figures show the recovered magnetic susceptibilities of the rocks with the values more than 0.01, 0.02, 0.03, 0.04, 0.05 SI, to the depth of 6 km, respectively. In this model the high magnetic susceptibility commonly related to volcanic units or mafic-ultramafic intrusive bodies. It is clear the high magnetic susceptibility zone in the SW of the area is related to Urumieh-Dokhtar magmatic belt.

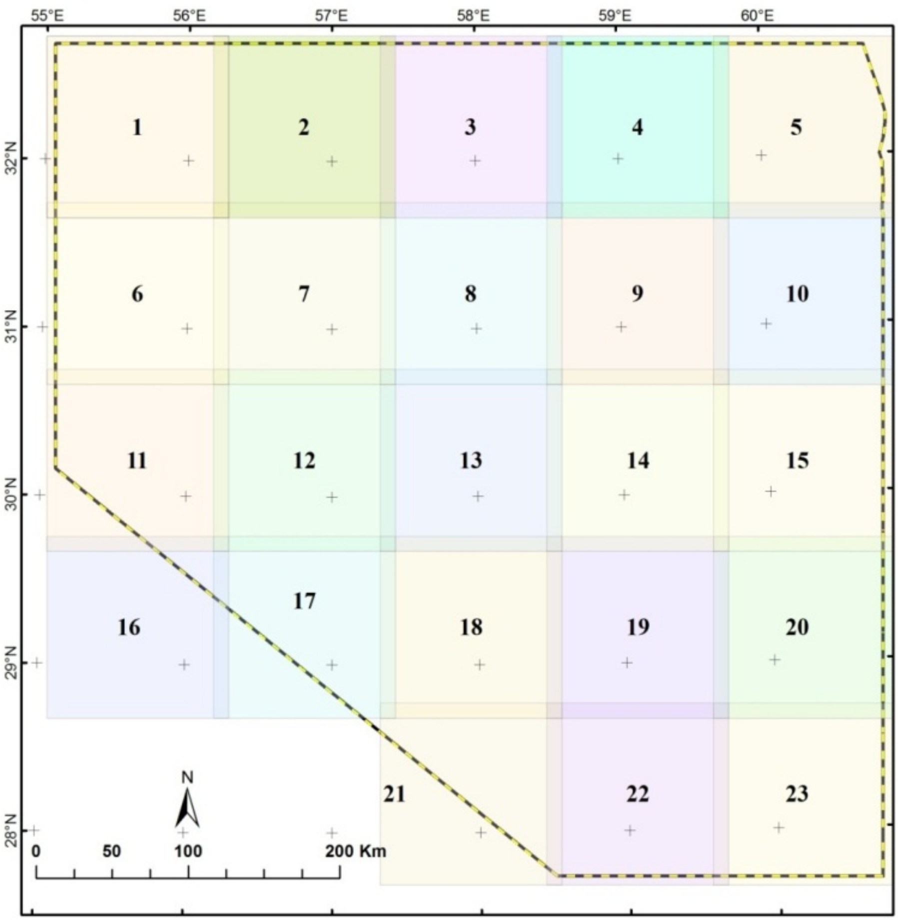

Fig. 5. Dividing of study area into 23 separated blocks with dimension of 120 × 120 km. The data were inverted separately in each block, and finally the inversion results were combined. To remove edge effects of the inversion, a 10 km overlap is considered for adjacent blocks, and initial parameters for modeling were chosen similar in all blocks.

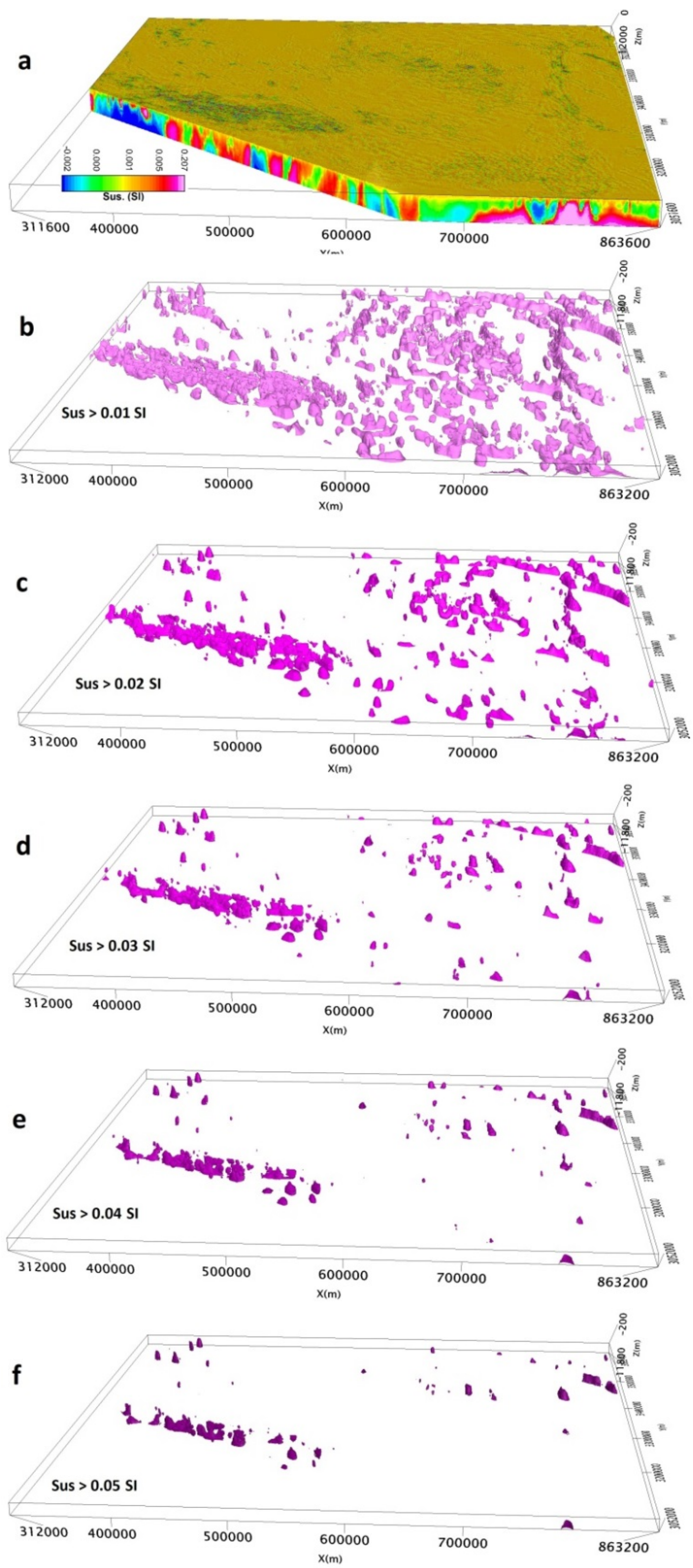

Fig. 6. 3D inversion of data from the surface to depth of 6 km using Li- Oldenburg algorithm (1998). a) the combined inverted magnetic susceptibility cells; b) magnetic susceptibility cutoff at more than 0.01 SI; c) 0.02 SI; d) 0.03 SI; e) 0.04 SI; f) 0.05 SI

3.5. Mapping of igneous rocks in Central Iran

3.5.1. Intrusive rocks

Intrusive rocks distributed throughout Iran, including Urumieh-Dokhtar magmatic Arc (UDMA), East Iranian Ophiolite Belt, Lut block, Robate-Poshte-Badamn are, and Saqand area. In the map of structural units of Iran, UDMA has a higher volume and extent. Rocks from this magmatic belt are considered to be related to continental margin magmatic arc. There are different views about the origin of magmatic rocks in Central Iran and East Block, such as intra-continental rift, subduction zone and back-arc extension. However, according to the structural and geological setting of Iran, rifting event play an important role in magmatic rocks formation. The age of the most intrusive rocks was estimated to be the Mesozoic Eocene and Tertiary. But some of them such as Khoshumi, Zarigan, Narigan granite in Robate-Poshte-Badam and Saqand blocks are related to the Precambrian and Cambrian.

Based on aeromagnetic data interpretation in the study area a number of 1215 concealed intrusive bodies were detected and delineated, which 531 igneous bodies were intermediate-felsic and 684 were mafic-ultramafic (Fig. 7). These bodies concealed in depth of low (from surface to 300 m), medium (300 to 1000 m) and high (more than 1000 m).

Outcropped intrusive bodies and the concealed ones in the study area can be classified in 10 zones based on the background geology: 1- UDMA, 2- Baft ophiolite belt, 3- Bazman area, 4- East Iran Ophiolite Belt, 5- west of Taftan Mountain, 6- Zahedan Granitoid Belt, 7- Northern Lut zone, 8-Eastern Lut zone, 9- Central Lut zone, 10- Southern Lut zone, 11- Poshte-Badam, and 12- Saqand.

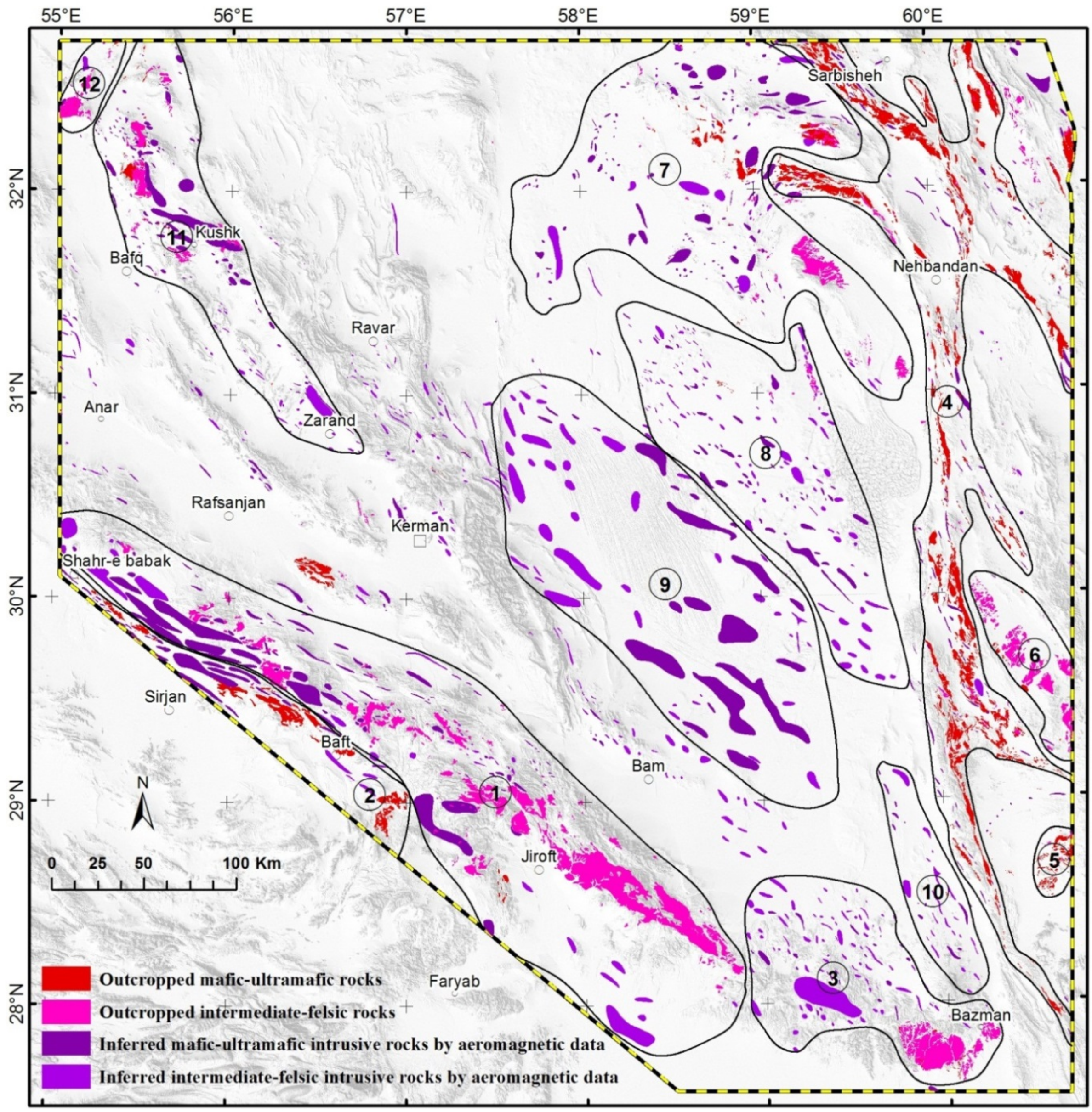

Fig. 7. Map of outcropped and inferred intrusive igneous rocks by aeromagnetic data. 1- Urumieh-Dokhtar Magmatic Arc (UDMA), 2- Baft ophiolite belt, 3- Bazman area, 4- East Iran Ophiolite Belt, 5- west of Taftan Mountain, 6- Zahedan Granitoid Belt, 7- Northern Lut zone, 8-Eastern Lut zone, 9- Central Lut zone, 10- Southern Lut zone, 11- Poshte-Badam, and 12- Saqand.

(1) Urumieh-Dokhtar Magmatic Arc

Urumieh-Dokhtar Magmatic Arc (UDMA), located in the active margin of Central Iranian Microcontinent, between Sanandaj-Sirjan zone and Central Iran block, is comprised mainly of tholeiite, calc-alkaline, and potassium-rich alkaline intrusive and extrusive rocks (Alavi, 1994; Shahabpour, 2007). The structure of UDMA is associated Neotethys subduction beneath Central Iran (Berberian and King, 1981). Oblique subduction of Neotethys beneath

Central Iran developed shear faults in the upper part of the crust and intrusion of granitoidic bodies. The type of intrusive rocks in this area is mostly comprised diorite, granite, and granodiorite (intermediate and acidic), which are related to the Oligocene. Aeromagnetic data interpretation revealed a number of 124 concealed intrusive bodies. The maximum variation of the magnetic field in study area is related to this belt (800 to 1200 nT). The high magnetic susceptibility (more than 0.05 SI) and strong magnetic response caused by high thickness of igneous rock units and different lithology in this zone. The large active mines such as Sarcheshme and Miduk are located in this zone.

(2) Baft ophiolite belt

Baft ophiolite belt is part of northwest-southeast trending Central Iran ophiolite belt, where is surrounded by UDMA in the north and Sanandaj-Sirjan metamorphic zone in the south. Baft ophiolite belt is mainly formed by closing of Naein-Baft oceanic basin (as a branch of Neotethys) during the Late Cretaceous (Arvin and Robinson, 1994). This ophiolite complex is a typical sequence including gabbro, serpentinized harzburgite, pillow lavas, dolerite dykes, limestone, tuff, keratophyre, and chert. In this belt, magnetic bodies are chiefly massive gabbro. Although, the most of this area is covered by recent deposits but the high magnetic susceptibility of buried mafic-ultramafic rocks caused to detect the concealed one easily. Aeromagnetic data interpretation detected and delineated a number of 66 concealed mafic-ultramafic intrusive bodies with dimension of about 492 km^2. Obviously, the magnetic field intensity is high with the average of 600 and maximum of 1500 nT, in the area. Magnetic data interpretation revealed the depth of the upper surface of detected concealed bodies is about low to medium.

(3) Bazman area

Bazman granitic body is located in the southern margin of Lut block along UDMA. This belt is the product of the closing of the neo-Tethys ocean in the south, beneath the southern margin of Lut block (Eurasia) in the north, in late cretaceous. Igneous rocks of the region are identified as I-type granitoids and volcanic island arc are indicated an active continental margin (Shahabpur, 2010). Aeromagnetic data interpretation and igneous units mapping revealed that there are many smaller intrusive bodies in NW of Bazman batholith, which is related to the magmatic activities of Bazman batholith. This region is characterized by a set of 99 isolated and discontinuous magnetic anomalies of the approximately 60-140 nT with regular shape of ellipses or linear. All of detected intrusive bodies are concealed and classified in the depth of low to medium.

(4) East Iran Ophiolite Belt

This belt strikes NS along Sistan suture zone in the east of Iran. There are different ophiolitic complexes along the Sistan suture zone which form a discontinuous NS trending belt from East of Bazman in the south to Birjand in the north indicating that the zone is the remains of an oceanic crust. It is believed the subduction of the oceanic crust between Lut and Afghan blocks during the late cretaceous played a major role in the tectonic evolution of this area (Tirul et al., 1983; Arjmandzadeh et al., 2011). Ophiolite massifs emerged into surface mainly through main faults, especially Nehbandan fault group. The northern terminal of this belt is divided into the branches, as a result of strike-slip fault activities. In the southern border the NS trends also inclined to the SW and continue to Pakistan. The composition of the outcropped ophiolite is mafic-ultramafic and mainly consists of peridotite, harzburgite, serpentinite, and other basic rocks. These rocks are easily detectable in the covered area, regarding the high magnetic susceptibility of mafic-ultramafic rocks. This belt corresponds to mainly NS aeromagnetic anomaly zone along which there are about 300-400 nT linear anomalies with a gradient of 100-300 nT/km and 150-300 nT/km on the vertical first derivative and analytical signal map, respectively. A number of 133 concealed mafic-ultramafic intrusive bodies were detected and mapped in this belt.

(5) West of Taftan Mountain

The ophiolite massifs of the west of Taftan are the base of batholithic massif of Taftan volcano. According to the map of magnetic field, magmatic belt of Taftan region is 75 km in length and 30 km in width, extends from the west of Taftan Mountain to a couple of kilometers inside the study area. The zone has an east-west trend, although magnetic anomalies show NW-SE trend. Only the western part of this magmatic belt is located inside the study area. The age of the massif like the other ophiolite massifs of Sistan block is related to the Cretaceous. Magnetic field variation in this zone is about 150-250 nT. Magnetic susceptibility of ophiolite massifs in the zone sound to be low, therefore just one concealed body is detected by aeromagnetic data in the depth of around 200-300 m.

(6) Zahedan Granitoid Belt

Zahedan Granitoid Belt is located in the southwest of Zahedan and extends about 100 km toward SE direction. This complex is included granite, granodiorite, and diorite rocks which is intruded into flysch sedimentary host rocks, during Eocene. Therefore, Zahedan granitiod is not product of the subduction of Lut or Afghan blocks. This belt is non-magnetic in RTP map. According to the magnetic susceptibility measured by Sadeghian and Valizadeh (2008) on 590 samples from this granitic complex, granite rocks are paramagnetic with average susceptibility below 0.0005 SI, whereas diorite rocks are ferromagnetic with average susceptibility more than 0.0005 SI.

(7) North of Lut zone

Lut block is placed between two NS main faults of Nayband and Nehbandan. The pressures were applied on the area have caused the strike-slip and shear types of displacements along these faults. In such systems, the volcanic eruption was intense and continuous, and younger lavas have successively covered the former rocks and formed extensive volcanic rocks of the block (Nogol-Sadat, 1993). This zone is characterized by short wavelength and strong amplitude magnetic anomalies of approximately 500-1000 nT. The outcropped intrusive rocks of the zone are less than the volcanic rocks; so the magnetic field response is wide and varied. Magmatic activities started from 77 Ma ago during the Late Cretaceous and lasted for five years. Magmatic rocks lithology is basaltic, andesitic, dacitic, and rhyolitic lavas, as well as less semi-deep intrusive rocks.

A number of 176 concealed mafic-ultramafic, and intermediate to acidic intrusive rocks were detected and delineated in Northern Lut zone. With exception of a few cases, aeromagnetic anomalies spread irregularly with no distinctive trend. Aeromagnetic anomalies, affected by Sistan suture branches, rotated counterclockwise from NW-SE trend to NE-SW in the east part of the zone. Anomalies trend is NS, close to Nayband Fault in the west part of the zone; trend of this faulted zone caused strong aeromagnetic anomalies extended to tens of kilometers on the surface. Generally, low anomalies from the shallow depth in the crust are detectable in this zone. Detected concealed rock bodies have dimension of 1128 km. Since magnetic volcanic rocks spread extensively throughout the area, are superimposed on the background of intrusive rocks, make it difficult to identify them. In such cases application of upward continuation (100 to 1000 m upward) are weakening the surficial anomalies. Aeromagnetic map and 3D inversion data revealed that the most of concealed rock bodies are shallow and moderate (less than 1000 m). Main mines like Ghale Zari copper mine formation is related to such magmatic activities.

(8) Eastern Lut zone

As it mentioned earlier, shear movements of both faults of Nehbandan in the east and Nayband in the west prevail an extensional condition in Lut block provided the possibility of intrusion for igneous rocks. Detected many concealed intrusive rocks in the area are evidences of this claim. The intrusive rocks in the Eastern Lut Zone are featured by irregular variations on the magnetic map from 100 to 300 nT and with some up to 800 nT. By analyzing the magnetic data, the strikes of newly mapped intrusive rocks are NW trending, which were strictly controlled by regional structure. A total number of 158 mafic to acidic intrusive rocks with dimension of more than 900 km^2 have been detected. According to the inversion of data, the depth of the intrusive bodies is mainly medium (300 to 1000 m) and some of them are estimated to be deep (more than 1000 m).

(9) Central Lut zone

Central Lut zone is covered by the recent sediment; therefore the geophysical data is the only way to study the zone. Magnetic data optimally delineate the buried magnetic rocks. The map of magnetic field shows long wavelength and medium amplitude anomalies probably originated from deep magnetic rocks. The main difference between Central and Eastern Lut zone is the deeper burial depth of igneous rocks in the former. The general trend of anomalies is relatively NW-SE with 100 to 200 nT. A total number of 67 intrusive rocks with dimension of 3130 km^2 is detected and delineated there. Aeromagnetic data interpretation revealed the burial depth of more than 1000 m for the most of concealed magnetic intrusives. The northern and southern have of intrusive rocks are classified compositionally into intermediate-felsic and mafic-ultramafic respectively.

(10) Southern Lut zone

In the southwestern margin of Lut block in the north of Bazman, there are a magmatic belt with remarkable anomaly and a unique trending which neither similar to ophiolite complex of Nehbandan Fault nor with the magmatic complex of Bazman Mountain. Regarding the spatial proximity with the magmatic complex of Bazman, the area probably was affected by Oman plate subduction beneath Lut block, melting of subducting lithosphere and the magma intrusions subsequently. The belt has a length of 130 km with NW-SE trend, is covered by sandstone and marl sedimentary rocks as well as volcanic silici-clastic sediments and except for a limited outcrop of gabbro in the center of the zone, no other outcropped intrusive rocks is visible. A number of 33 concealed magnetic intrusive rocks, estimated to be in medium depth (300 to 1000 m), are revealed by magnetic evidence. Most of the intrusive rocks are at the same direction with the regional trend (NW-SE) compositionally are intermediate to felsic with some mafic.

(11) Poshte-Badam

Bafgh-Saqand region (Poshte-Badam block) is a significant matallogenic province in Iran with major mineralization such as iron deposit (Choqart, Chadormalu, Sechahun, Lake-Siah, Mishdvan, Chah Gaz, and etc.), phosphate deposit (Esfordi, Zarigan, and Gazestan), copper and zinc (Koushk and Gazestan), lead and zinc deposit (Kushk and Gazestan). Geology and aeromagnetic data of the region has been subjected to study by many researchers (Haghipour, 1974; Förster and Jafarzadeh, 1994; Ramazani & Tucker, 2003; Jami, 2005; Mokhtari & Emami, 2008; Torab, 2010; Bonyadi et al., 2011). The region has strong magnetic anomalies so that the maximum of aeromagnetic field variations reaches to 3000 nT. One of the significant features of the magnetic anomalies in Poshte-Badam zone is the presence of the strong corresponding negative and positive poles in TMI map, which is related to magnetite mineralization. This feature in aeromagnetic map is applied for fast tracing and detecting of shallow and deep magnetite deposits. Acidic intrusive rocks with low magnetic intensity are also common in the region such as Zarigan and Chah-chule Granitic bodies in north of Bafgh and Hamijan and Ferdos granitic bodies in SW of Bahabad. Samani (1998) believed that all of the magnetite and granitic bodies in this zone have been originated by metasomatism processes. A total of 153 concealed intrusive bodies mostly mafic-ultramafic were detected. Based on magnetic data interpretation and mapping, the most intrusive rocks are from northeast of Bafgh at the vicinity of granitic massifs of Zarigan and Hamijan. Detected rocks bodies are in different depth but most of them are estimated in the depth of medium (300 to 1000 m). The intrusive rocks in the southern and northern parts of the area are classified mostly into acidic-intermediate and mafic-ultramafic respectively.

(12) Saqand

Saqand region is located in Central Iran Microcontinent between two main faults of Poshte-Badam and Chapedony. In this zone, the main known outcropped intrusive rocks is Kheshumi-Dare Anjir intrusive complex which is located in the south. This complex including two related intrusive bodies: Kheshumi Granite and Dare Anjir Diorite with low to moderate magnetic response that are consist of many intruded Eocene dykes with moderate to high magnetic response. This zone is relatively non-magnetic to low magnetic with the magnetic field average variation of 100 nT. Only 6 concealed intrusive rocks (5 intermediate to felsic and 1 mafic) at the depth of medium are detected and mapped.

3.5.2. Volcanic rocks

Volcanic rocks in Iran have significant expansion and thickness, particularly in UDMA, Central Iran, and Lut block. Most of these volcanic rocks are related to Eocene to Tertiary. It seems with the compressional movements and related heat follows caused by the Late Cretaceous event (Laramide orogeny), extensive magma generations of volcanic lavas and pyroclastic caused by global extension phase was the most during the Eocene, and repeated during the Early Oligocene (37-40 Ma), the Middle Miocene (19-22 Ma), and the Pliocene (12 Ma); the recent active and semi-active volcanoes of Iran are the continuation of theses magmatic events (Darvishzadeh, 1990). Extended areas of concealed volcanic rocks were detected and delineated based on aeromagnetic data interpretation. Figure 8 illustrated the map of the outcropped and concealed volcanic rocks in study area. A total of 528 magnetic anomalies caused by volcanic rocks were revealed with dimension of 20000 km^2. Most of the concealed volcanic rocks are in UDMA and Lut block. It should be noted that the new detected concealed volcanic rocks are mostly outcropped or near surface and should not be considered as deep rocks, because a magmatic rock unit is considered as an extrusive igneous rock (volcanic), when it reaches to surface. Since the observation of irregular anomalies with high frequency and high amplitude on magnetic map is one of the main criteria in detection of concealed volcanic rock. The volcanic rocks buried in high depth or covered by a massive thickness of sediments show regular anomalies with low frequency which make those hard to detection by aeromagnetic data. The upper surface of detected concealed volcanic rocks is estimated to be shallow (less than 300 m) or medium (300 to 700 m).

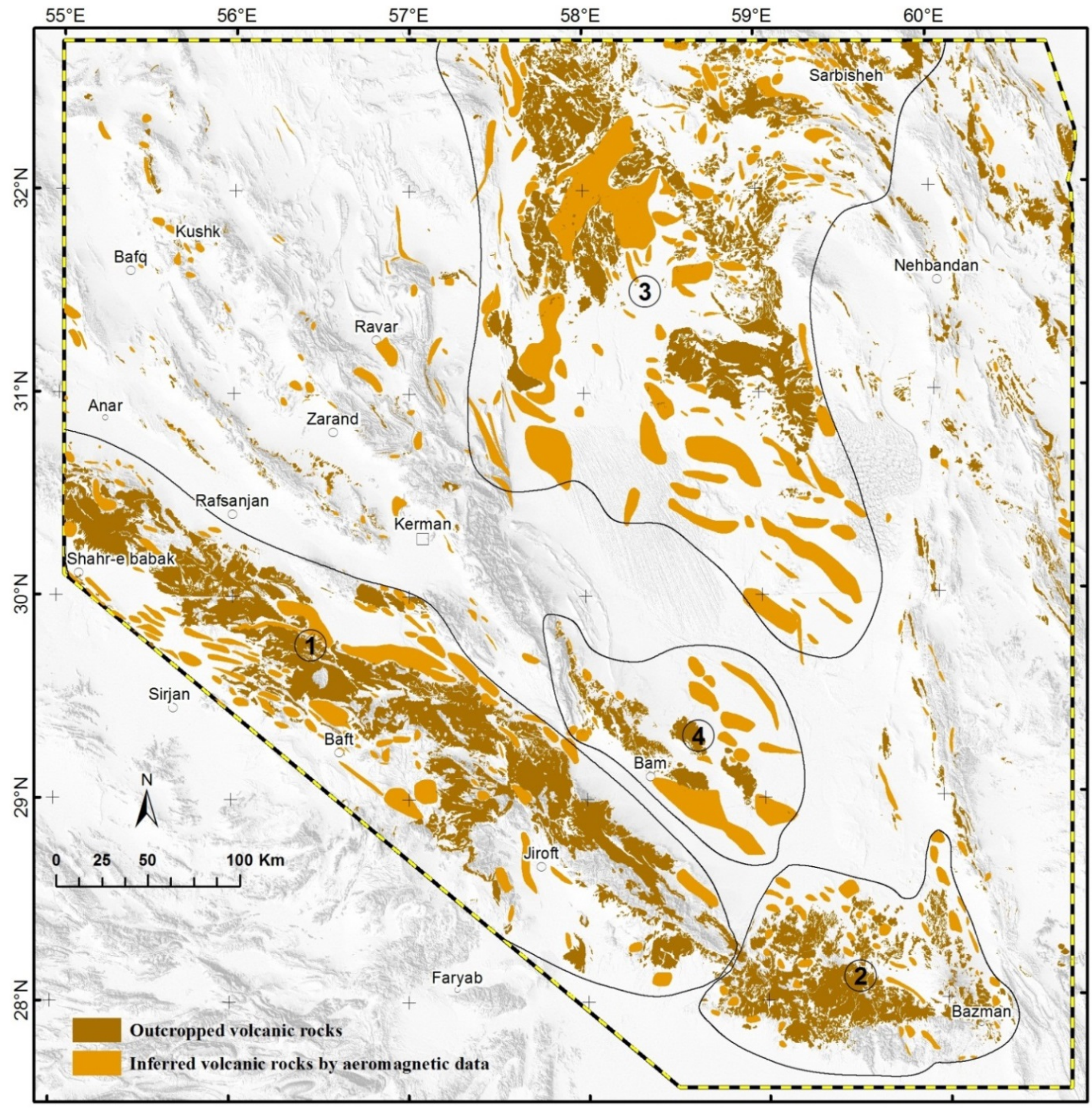

Fig. 8. The distribution map of volcanic rocks based on the field observation and aeromagnetic data. 1- Urumieh-Dokhtar volcanic belt, 2- Bazman volcanic zone, 3- Northern Lut volcanic zone, 4- Bam Volcanic zone

(1) Urumieh-Dokhtar volcanic belt

Extensive magmatic activities of Urumieh-Dokhtar volcanic belt took place during the Paleocene–Eocene and the Middle-Late Eocene in particular along with the latest subduction event of Neotethys oceanic lithosphere beneath Central Iran during the Upper Cretaceous. There are different hypothesis on this magmatic activity. Most researchers considered magmatic activity of Urumieh-Dokhtar belt during Tertiary as the continental margin island arc. Magnetic features of the zone are strong and numerous that the anomalies are still prominent in magnetic maps upward a few kilometers. Generally, magnetic anomalies in this belt are linear with NW-SE trend. The most volcanic outcrops are andesite, dacite, basalt, trachyandesite and tuff. They have a medium magnetic susceptibility, therefore the extensive thickness and volume of volcanic rocks is the main reason of strong magnetic anomalies in this zone.

(2) Bazman volcanic zone

Bazman volcanic zone is located in the southeast of Iran, 111 km NW of Iranshahr. This volcanic cone belongs to Central Iran in the SE margin of Lut block. Bazman's main cone is a stratified volcano whose lava flows out of several craters. This volcano has a complex structure and composed of different types of lavas including andesite, dacite, and rhyodacite especially in the eastern apron. Main cone is a series of alternating ignimbrite, pumice, and lava breccia. This complex is magmatic island arc (continental active margin) according to the lithology, mineralogy, and geochemistry (Shahabpur, 2010). Considering to the current position of Bazman volcano and occurrence of volcanic rocks in the north and the northwest, magmatic activities appear to be concentered in the NW of the zone and gradually moving to the east and southeast. Linear anomalies with NW-SE trend in Bazman area are a significant tectonic feature on the magnetic map of area with bigger NS component than Urumieh-Dokhtar belt. The average of magnetic field variation is 300 nT showing intermediate lithology.

(3) North Lut volcanic zone

As mentioned earlier, the extensional condition dominated in Lut block due to shear movements of Nehbandan and Nayband faults widely provide the suitable conditions for magmatic activity particularly in the northern part. The magmatic activities started at the Late Cretaceous (77 Ma) and lasted for 5 Ma. There are more than 40 volcanic cones in this block (Darvishzadeh, 1990). Magmatic rocks are basalt, andesite, dacite, and rhyolite lavas as well as less medium depth intrusive rocks. In the southern part of the zone that correlated with central parts of Lut block, with increasing the thickness of the recent sediments and covering the rock units, noticeable volcanic rocks have been detected and delineated based on magnetic data interpretation. The volcanic activity of Lut block seems to have extended to about 70 km south of the present outcrops, which may be covered by the recent sediments. Magnetic field variation range from $n \times 100$ to $n \times 1000$ nT.

(5) Bam Volcanic zone

In the southwestern margin of Lut block, volcanic rocks of basalt and tuff are observed, mostly enclosed in Bam fault zone. The controlling factor of these units seem to be the main branches of Bam fault zone which are extended along with Urumieh-Dokhtar belt; even so the magnetic line trend have more northern component in Bam zone. Magnetic anomalies range about 100 to 300 nT. Concealed parts of the volcanic rocks in the zone are detected and delineated based on the magnetic data interpretation. Some of these concealed volcanic rocks are located in the south and others are located in the east of volcanic outcrops as well as the southwestern margin of Lut block.

4- Conclusion

According to aeromagnetic data interpretation, this work helps to characterize the distribution of igneous rocks in Central Iran Microcontinent. Usually, the traditional method such as field observation can hardly define concealed or buried igneous rocks, but the magnetic data could compensate for this deficiency. However, when anomalies of very low-magnetic or non-magnetic igneous rocks are superimposed on the background of non-magnetic units, the aeromagnetic anomaly is unavailable. Magnetic data processing and results of 3D inversion of data combined with the geological information revealed the concealed igneous activities in Central Iran. In the present study a total number of 1215 concealed mafic to felsic intrusive igneous rocks and 528 unknown volcanic rock units are detected and delineated. Concealed intrusive rocks and the known intrusive rocks on the geological maps were analyzed together and divided into 12 basins of intrusive magmatism, based on the structural and tectonic settings. Each of these basins was analyzed in terms of structure and depth of the concealed rock bodies. The same processes accomplished on the volcanic rock units and 4 volcanic basins were studied. The results show the southern part of Lut block is very dynamic regarding magmatic activity, so that it could be noteworthy for the mining exploration.

Acknowledgement

References

Abdelsalam, M.G., Katumwehe, A.B., Atekwana, E.A., Le Pera, A.K., Achang, M., 2016. The Paleoproterozoic Singo granite in south-central Uganda revealed as a nested igneous ring complex using geophysical data. J. Afr. Earth Sci. 116, 198–212.

Alavi, M., 1994. Tectonics of Zagros Orogenic Belt of Iran, New Data and Interpretation. Tectonophysics 229, 211-238.

Anudu, G.K., Stephenson, R.A., Macdonald, D.I.M., 2014. Using high-resolution aeromagnetic data to recognise and map intra-sedimentary volcanic rocks and geological structures across the Cretaceous middle Benue Trough, Nigeria. J. Afr. Earth Sci. 99, 625–636

Arjmandzadeh, R., Karimpour, M.H., Mazaheri, S.A., Santos, J.F., Medina, J.M., & Homam, S. M., 2011. Two-sided asymmetric subduction; implications for tectonomagmatic and metallogenic evolution of the Lut Block, eastern Iran. J. Econ. Geol. 1, 3, 1-14.

Arkani-Hamed, J., 2007. Differential reduction to the pole. Geophysics Journal International 72, 13–20.

Arvin M., Robinson P.T., 1994. The petrogenesis and tectonic setting of lavas from the Baft ophiolitic mélange, southwest of Kerman, Iran. Canadian Journal of Earth Sciences 31, 824–834.

Alamdar, K., Ansari, A. H. and Kamkar A., 2012. Using analytic signal in determination of the magnetization to density ratio (MDR) of the geological bodies, journal of the Earth and Space Physics 38, 2.

Anudu, G.K., Stephenson, R.A., Macdonald, D.I.M., 2014. Using high-resolution aeromagnetic data to recognise and map intra-sedimentary volcanic rocks and geological structures across the Cretaceous middle Benue Trough, Nigeria. J. Afr. Earth Sci. 99, 625–636.

Barnov, V., 1957. A new method for interpretation of aeromagnetic maps: Pseudo-gravimetric anomalies. Geophysics, 22, 359-383.

Barrier, E., Vrielynck, B., 2008. Paleotectonic Maps of the Middle East, Middle East Basins Evolution Programme (Atlas of 14 Maps). CCGM-CGMW, Paris.

Behrendt, J.C., 2013. The aeromagnetic method as a tool to identify Cenozoic magmatism in the West Antarctic Rift System beneath the West Antarctic Ice Sheet-A review; Thiel subglacial volcano as possible source of the ash layer in the WAISCORE. Tectonophysics 585, 124–136.

Berberian, M., King, G.C.P., 1981. Towards a paleogeography and tectonic evolution of Iran. Canadian Journal of Earth Sciences 18, 210–265.

Bonyadi, Z., Davidson, G.J., Mehrabi, B., Meffre, S. and Ghazban, F., 2011. Significance of apatite REE depletion and monazite inclusions in the brecciated Se-Chahun iron oxide-apatite deposit, Bafq district, Iran: Insights from paragenesis and geochemistry, Chemical Geology, 281, 253-269.

Brunet, M.-F., Wilmsen, M., Granath, J.W. (Eds.), 2009. South Caspian to Central Iran Basins: The Geological Society Special Publications, 312, 1–6.

Chernicoff, C.J., Zappettini, E.O., Santos, J.O.S., Godeas, M.C., Belousova, E., McNaughton, N.J., 2012. Identification and isotopic studies of early Cambrian magmatism (El Carancho Igneous Complex) at the boundary between Pampia terrane and the Río de la Plata craton, La Pampa province, Argentina. Gondwana Res. 21, 378–393.

Clark A., 1997. Magnetic petrophysics and magnetic petrology: Aids to geological interpretation of magnetic surveys, J. Australian geology & geophysics 17, 2, 83-103.

Darivishzadeh, 1990, Geology of Iran. Amirkabir Publications, 901p.

Emami, M. H., Sadeghi, M. M., Omrani, S. J., 1993. Magmatic map of Iran (Tehran). Geol. Surv. Iran.

Farr, T.G., Rosen, P.A., Caro, E., R. Crippen, R., Duren, S., Hensley, M., Kobrick, M., Paller, E., Rodriguez, L., Roth, D., Seal, S., Shaffer, J., Shimada, J., Umland, M., Werner, M., Oskin, D., Burbank, Alsdorf, D., 2007. The shuttle radar topography mission. Rev. Geophys. 45, 2.

Fedi, M., Florio, G., Rapolla, A., 1994. A method to estimate the total magnetization direction from a distortion analysis of magnetic anomalies. Geophysical Prospecting, 42, 261-274.

Finn, C.A., Morgan, L.A., 2002. High-resolution aeromagnetic mapping of volcanic terrain, Yellowstone National Park. J. Volcanol. Geoth. Res. 115, 207–231.

Förster, H.J. and Jafarzadeh, A., 1994. The Chador Malu iron ore deposit, Bafq district, Central Iran, magnetite filled pipes: neues jahrbuch für geologie und paläontologie monatshefte, 168, 524-534.

Galindo-Zaldívar, J., Ruiz-Constán, A., Pedrera, A., Ghidella, M., Montes, M., Nozal, F., Rodríguez-Fernandez, L.R., 2013. Magnetic anomalies in Bahia Esperanza: a window of magmatic arc intrusions and glacier erosion over the northeastern Antarctic Peninsula. Tectonophysics 585, 68–76.

Gansser, A., Gupta, H.K., Delany, F.M., 1981. The geodynamic history of the Himalaya, Zagros, Hindu Kush, Himalaya; geodynamic evolution. Geodynamics Series 3, 111–121.

Gunn, P.J., 1997. Application of aeromagnetic surveys to sedimentary basin studies. J. Aust. Geol. Geophys. 17, 133–144.

Haghipour, A., 1974. Etude geologique de la region de Biabanak- Bafq (Iran Central), Pour obtenir le grade de Docteur es sciences natureles.

Jami, M., 2005. Geology, geochemistry and evolution of the Esfordi phosphate- iron deposit, Bafq area, Central Iran, Unpublished Ph.D. thesis, University of South Wales, 403p.

Jarvis, A., Reuter, H.I., Nelson, A., Guevara, E., 2008. Hole-filled SRTM for the Globe Version 4. available from: the CGIAR-CSI SRTM 90m Database.

Li, Y., Oldenburg D.W., 1996. 3D inversion of magnetic data. Geophysics 6, 394–408.

Louro, V.H.A., Mantovani, M.S.M., 2012. 3D inversion and modeling of magnetic and gravimetric data characterizing the geophysical anomaly source in Pratinha I in the southeast of Brazil. Journal of Applied Geophysics, 80, 110-120.

Mietha, M., Jacobs, J., Ruppel, A., Damaske, D., Läufer, A., Jokat, W., 2014. New detailed aeromagnetic and geological data of eastern Dronning Maud Land: implications for refining the tectonic and structural framework of Sør Rondane, East Antarctica. Precambr. Res. 245, 174–185.

Mohammadzadeh, M., Mirzaei, S., Nouraliee, J., Porkhial, S., 2016. Integrated magnetic and gravity surveys for geothermal exploration in Central Iran, Arab J Geosci, 9:506.

Mokhtari, M.A., Emami, M.H., 2008. REE pattern and REE mineralization in apatite-magnetite deposits of Bafq Saghand district (Central Iran), Geosciences, Scientific Quarterly Journal, Special Issue, 17, 162-169.

Muttoni, G., Mattei, M., Balini, M., Zanchi, A., Gaetani, M., Berra, F., 2009. The drift history of Iran from the Ordovician to the Triassic. South Caspian to Central Iran Basins. Geological Society, London, Special Publications 312, 7–29.

Nogole-Sadat, M.A., 1993. Tectonic Map of Iran, Geological Survey of Iran 1:1,000,000 scale.

Oldenburg, D. W., and Pratt, D.A., 2007. Geophysical inversion for mineral exploration - A decade of progress in theory and practice, in B. Milkereit, ed., Proceedings of Exploration 07: Fifth Decennial International Conference on Mineral Exploration, 61–95.

Oskooi B., Mirzaei M., Mohammadi B., Moghaddam M.M., Ghadimi F., 2016. Integrated interpretation of the magnetotelluric and magnetic data from Mahallat geothermal field, Iran. Stud Geophys Geod 60, 141–161.

Ramazani, J. and Tucker, R.D., 2003. The Saghand region, Central Iran: U-Pb geochronology, petrogenesis and implications for Gondwana tectonics, American Journal of Science 303, 622-665.

Sadeghian, M., Valizadeh, M., 2008. Emplacement Mechanism of Zahedan Granitoidic Plutonwith the Aid of AMS, Geosciences, 17, 66, 134-159.

Samani, B., 1998. Precambrian mineralization in Central Iran, Journal of Nuclear organization of Iran, 17, 1-16.

Shahabpour, J., 2007. Island-arc affinity of the Central Iranian volcanic belt. International Journal of Asian Earth Sciences, 30, 652–665.

Shahabpour, J., 2010. Tectonic implications of the geochemical data from the Makran igneous rocks in Iran, Island Arc 19, 4, 676–689.

Stöcklin, J., 1968. Structural history and tectonics of Iran: a review. AAPG52, 7, 1229–1258.

Sengör, A.M.C., 1987. Tectonics of the Tethysides: Orogenic Collage Development in a Collisional Setting. Annual Review of Earth and Planetary Sciences 15, 213–244.

Sengör, A.M.C., 1990. Plate Tectonics and Orogenic Research After 25 years; a Tethyan Perspective Earth Science Reviews, 27. Elsevier Science Publishers, 1–201.

Stampfli, G., Borel, G.D., 2002. A plate tectonic model for the Palaeozoic and Mesozoic constrained by dynamic plate boundaries and restored synthetic oceanic isochrones. Earth and Planetary Science Letters 196, 17–33.

Stille, H., 1910. Die mitteldeutsche Rahmenfaltung. Jahresbericht des Niedersächsischen Geologischen Verein 3, 141–170.

Tirrul, R., Bell, I.R., Griffis, R.J. & Camp, V.E., 1983. The Sistan suture zone of eastern Iran. Geol. Soc. Am. Bull. 94, 134–150.

Torab, F.M., 2010. Geochemistry and radio- isotope studies on the iron- apatite ores in Bafq metalogenic zone for determination of apatite origin: Iranian Journal of Crystallography and Mineralogy 18, 3, 409-418.

Xu, X.K., Liu, S., Shi, H.X., Xu, G.Q., Zhou, W., 2009. The hydrocarbon geology conditions of Kashan area in central Iranian basin. J Southw Pet Univ (Sci Technol Edn) 7, 62–68.
Kheyrollahi, H., Alinia, F., Ghods, A., 2018. Regional magnetic lithologies and structures as controls on porphyry copper deposits: evidence from Iran, Exploration Geophysics, 49, 1, 98-110.

Xiong, S., Yang, H., Ding, Y., Li, Z., Li, W., 2016. Distribution of igneous rocks in China revealed by aeromagnetic data, Journal of Asian Earth Sciences 129, 231–242.

Zhu, Y., 2013. Geotectonic and Deep Structures in China-Preliminary Interpretation of National 1:1000000 Aeromagnetic Maps. Geological Publishing House, Beijing, p. 252 (in Chinese).

Dear Editor and Reviewers

Thank you for your consideration to our manuscript. We consider all comments and reply to each comments as following. At first, we prefer to state some general explanations.

This research is results of several years of works of geological and geophysical groups in geological society of Iran and several consulting companies which archived their studies by unpublished reports and data. We hope this paper becomes a reference for future related studies. We are a little surprised by concerning and commenting of reviewers about some parts of the manuscript. Although we believe this concerning can be exist in the study, but it sounds be normal for each indirect study method. In this study we only use one method (aeromagnetic) for revealing underground structures and obviously for precious information we need more data and information such as complementary geophysical methods and borehole data which is not exist yet. Fortunately in the current study we used semi-high resolution aeromagnetic data (Line spacing: 1000 m) which is not used in any similar paper. The recently published paper by Teknik et al. (2020) is used the historical low-resolution aeromagnetic data (Line spacing: 7.5 km). They are presented only a calculated susceptibility map without introducing concealed/new igneous units. They only illustrated previous mapped igneous units (Published by GSI) and compared with the calculated magnetic susceptibility. But in the submitted article, we produced two new maps of known and concealed igneous units based on high-resolution aeromagnetic data, analyzed measured susceptibility data and geological information.

The other concern of reviewers is related to the analyzed magnetic susceptibility measurements and their interpretation. They state there are some exceptions for susceptibility of igneous rocks. Although we accept this state and believe that the magnetic susceptibility is not a unique method for detection and classification of rocks, but generally based on magnetic susceptibility studies in whole of the world and Iran, the value of magnetic susceptibility of mafic rocks is bigger than of intermediate and felsic rocks or sedimentary rocks. So the magnetic susceptibility studies can be an effective tool for detection of igneous rocks and their general types (i.e mafic, intermediate, felsic), especially when the results be integrated with the geological information of interpreter. In the current study, qualitative interpretation of magnetic maps, amplitude and frequency of magnetic data, direct measurements of susceptibilities of igneous rocks, geological information of the surface and tectonic zone of study area are tools for detection and classification of igneous rocks.

1. The original map of magnetic anomalies used as a basis for the performed study is not given. Instead, the RTP map of the area is shown. Since the construction of this map is not a simple procedure and its accuracy is always questionable, the correct result can be obtained only provided that the anomalous magnetic field is influenced predominantly by inductive magnetization. For this reason, the authors use the original map of the anomalous field in their study. However, they do not give it. It would be better if they presented this map in the paper.

As you mentioned, many of interpretation are possible only by TMI map. So this map is presented in the paper.

2. The recently published paper by Teknik et al. (2020) (see References below) has much in common with the submitted manuscript both in the study area and in the subject of study, namely, the distribution of magmatic manifestations by anomalous magnetic field within the Iran area. The paper is based on the map of aeromagnetic anomalies (scale of 1:1,000,000) given by Saleh (2006) (see References below). The authors of the submitted manuscript do not mention this paper. They should have made a brief comparative analysis of their research and this paper, because there are many inconsistencies in their starting materials and conclusions, namely:
a) The magnetic field maps given in the two works differ significantly. Mind you, the submitted manuscript presents only the RTP field.

The magnetic field map in the two works is completely similar. But as described in data settings of each paper, the aeromagnetic data used in paper Teknik (2020) by Saleh (2006) is low resolution data with line spacing 7.5 km and flight height of 300-600m. But data used in our paper is semi-high resolution data with line spacing about 1000m and flight height of 120m.
Below figure is compared two mentioned data set. As can be seen, many of detailed anomalies are detectable in our map.

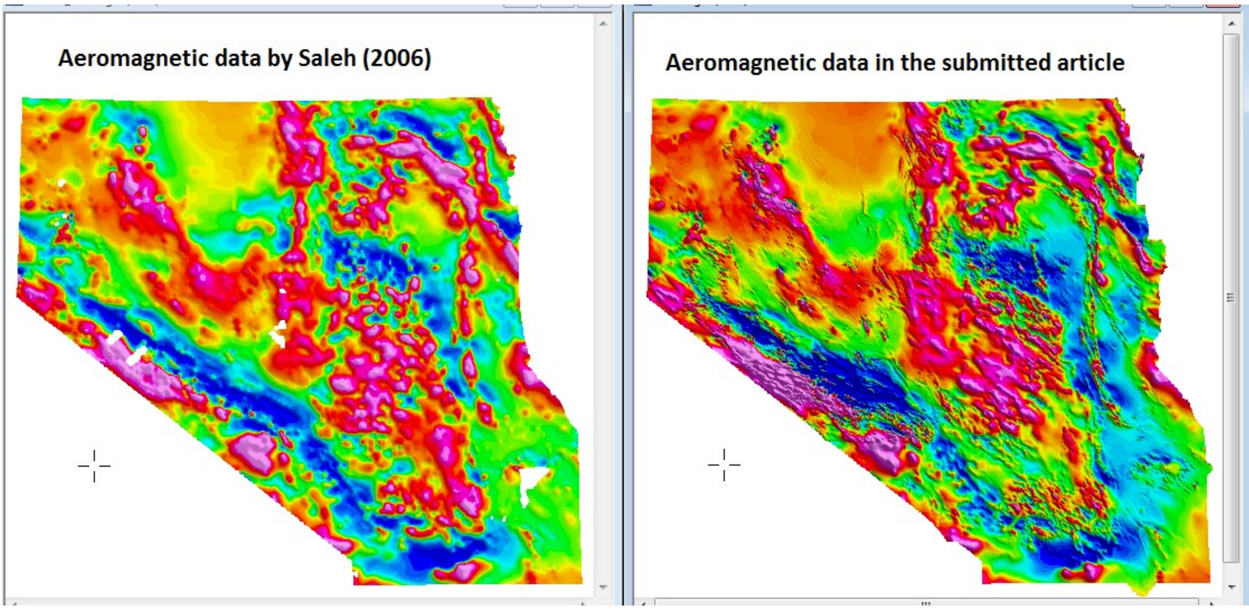

b) The classification of igneous rocks by magnetic properties differs strongly; the limiting values of magnetic susceptibility differ 1.5 times.
c) The distribution maps of different types of igneous rocks also differ noticeably.

Igneous rocks shown in fig.7 in paper Teknik et al. (2020) and presented outcropped igneous rocks in our work (Fig.7 and 8) are completely similar. Because both works used the same geological raster data file published by Geological Society of Iran (GSI). So, the observed difference in maps of two works is due to following reasons: 1- We presented the new detected igneous rocks and mapped ones in figs. 7 and 8, but they (Teknik et al, 2020) only presented outcropped igneous rocks, 2- Some differences are related to the classification procedures of igneous rocks; for example we classified ophiolitic rocks as mafic- ultramafic group while they

are classified ophiolitic rocks as a separated group and 3- We also renewed the boundaries of tens outcropped igneous rocks.
For more information of reviewers, we attached the shape file of igneous rocks, distributed by GSI. The classification of units is performed by us (see channel "Type" in the shape file).

3. The authors repeatedly claim a direct relationship between the composition of rocks and their magnetic susceptibility. However, this thesis is not correct in principle. The main minerals composing mafic rocks are usually weakly magnetic. The high magnetic susceptibility of mafic rocks is due to accessory ferrimagnetic minerals (for example, magnetite and titanomagnetite). Such minerals can also be present in salic (felsic) rocks (for example, alkali granites and alkali syenites), sometimes being responsible for their high magnetic susceptibility.

We agree that there are some exceptions in magnetic susceptibility of composition of rocks, but based on magnetic susceptibility studies in whole of the world and Iran, the value of magnetic susceptibility of mafic rocks is bigger than of intermediate and felsic rocks or sedimentary rocks. Susceptibility is the ratio of the strength of the induced magnetism to the strength of the field that caused it. Magnetic susceptibility depends largely on a rock's magnetic mineral content. Mafic rocks generally have higher magnetic susceptibilities than felsic rocks because <u>mafic rocks are typically more abundant in strongly magnetic minerals</u> such as magnetite (Carmichael, 1982).

Carmichael, R. S., 1982, Magnetic Properties of Minerals and Rocks: CRC Handbook of Physical Properties of Rocks, Vol. 2, Ch. 2.

4. The algorithm for dividing the found magnetic rocks into types is not described in detail and thus is not clear. Apparently, the main parameters used for rock typification are the magnetic susceptibility and shape of the rock bodies, but there are a number of objections to this typification:
a) It is impossible to determine unambiguously the particular type of rock according to its magnetic susceptibility, because the chemical composition of rock indirectly defines its magnetic properties.
b) The authors use the term "an average magnetic susceptibility" without specifying its meaning. If taking it literally, one can use this parameter for classification only in the case of unimodal normal distributions. The histograms of the occurrence of the magnetic properties of igneous rocks are usually strongly different from the Gauss curve (Dortman, 1984) (see References below). Moreover, bimodal distributions are also possible (for example, for salic rocks); in this case, the average magnetic susceptibility of rock might not characterize its type at all, because there are virtually no (or very few) such rocks with the average value of this parameter.

Magnetic susceptibility study is not unique our way for detecting of type of rocks, so an integrating of information is applied for this case. Maybe mentioned challenge in item 5 is related this case. In the current study, qualitative interpretation of magnetic maps, amplitude and frequency of magnetic data, direct measurements of susceptibilities of igneous rocks, geological information, tectonic block, surrounding geology, unpublished report of local areas and etc. are tools for detection and classification of igneous rocks.
Using the term of "an average magnetic susceptibility" is a common way for describing igneous rocks in whole of the world (Elizabeth et al., 2003(see the abstract), Yang et al., 2013 (see section 4-2) and Xiong, 2016 (some parts of the paper))

Elizabeth A. Sanger and Jonathan M. 2003. Density and Magnetic Susceptibility Values for Rocks in the Talkeetna Mountains and adjacent Region, South-Central Alaska, Open-File report 03-268, U.S. Geological Survey.

Yang, T., Gao, J., Gu, Z., Daga, B. and Tserenpil, B. 2013, Petrophysical Properties (Density and Magnetization) of Rocks from the Suhbaatar-Ulaanbaatar-Dalandzadgad Geophysical Profile in Mongolia and Their Implications, The Scientific World Journal, Hindawi.

Xiong, S., Yang, H., Ding, Y., Li, Z., Li, W., 2016. Distribution of igneous rocks in China revealed by aeromagnetic data, Journal of Asian Earth Sciences 129, 231–242.

c) The magnetic susceptibility obtained by inversion should be carefully used for rock typification, because the inversion algorithm yields smoothed solutions, i.e., a wide range of magnetic susceptibility values for a rock body, which decrease from its core to its periphery.
d) Note that a more complex model of the field sources (for example, the hypothesis of the different behavior of magnetic susceptibility with depth at different sites of the study area) can lead to different results of the inversion and their different interpretation. This should be given special attention in the paper.

Unfortunately non-uniqueness of solutions is a common problem for each unconstrained inversion method. Therefore, interpreter experience and geology information is a necessary prerequisite for a valid interpretation of study area.
For better use of the inverted model, we converted the calculated susceptibility data of each mesh to a point data including x,y,z and sus. Then, different cutoff of sus. and depths (z) was provided and exported to a shape file as a usable information layer in ArcGIS workspace.

5. A detailed comparison of Figs. 2, 7, and 8 reveals that many of the exposed igneous rocks shown in Figs. 7 and 8 are not displayed on the map of magnetic anomalies (Fig. 2) or, on the contrary, the anomalies shown in Fig. 2 are not depicted as magmatic manifestations in Figs. 7 and 8. This must be explained in terms of the method and technique used for the interpretation of magnetic anomalies.

As you mentioned as your main concern, magnetic susceptibility is not directly reflecting type of rocks, because there are some significant complicated relations between compositions of rocks and its magnetic response. Therefore, beside of magnetic data, geological information of the study area is necessary for a valid interpretation. In the current study, for places where the igneous rocks are outcropped, we used the mapped geological boundaries by GSI and for other places, the interpreter is decided if there is a covered igneous rocks near the surface and then recognized their types based on different magnetic maps, calculated susceptibility, tectonic block, surrounding geology and etc. as described in the article.

6. The paper by Arkani-Hamed (1998) mentioned in the text is absent from the list of references. It seems the year of its publication is wrong (maybe 1988?).

Arkani-Hamed (2007) is correct.

7. There are errors in Table 2:
a) A misprint (Table 1 instead of Table 2).

?!

b) Incorrect designation of magnetic susceptibility:
There must be (K, 10^{-3} SI) instead of (K10^{-3} SI).*

Corrected.

c) The upper values for felsic rocks are too high, and the upper value for magnetite is too low.

We revised the statistics of susceptibility values of intrusive rocks and modified the values for magnetite, syenite, granite and granodiorite by reclassification of max. and min. samples. There was no significant change in the mean values.

Table 1. Summary of regional data set.

Dataset	Data type	Data format	Actions
Geophysical	National Regional Aeromagnetic Data	Geosoft grids	Stitched individual grids and re-gridded to provide a continuous integrated grid
	1:250 000 interpretation of magnetic data contour sheets	Georeferenced images	None
	Ground-based gravity data processed by BGI	Geosoft grid	None
Geological	1:1000 000 Tectonic map of Iran	jpg image	Georeferenced. Mosaic and spatial join to form an integrated coverage
	1:1000 000 Magmatic map of Iran (Emami et al., 1993)	jpg image	Georeferenced. Mosaic and spatial join to form an integrated coverage
	1:250 000 Geology map sheets	jpg image	Georeferenced. Mosaic and spatial join to form an integrated coverage
	1:100 000 Geology map sheets	jpg image	Georeferenced. Mosaic and spatial join to form an integrated coverage
	1:250 000 Vector geology	Shapefile	Recoded data fields according to 1:250 000 map sheets
Satellite	Landsat (full individual scenes)	FST and geotiff	
	MrSID image	.sid (raster file)	
	SRTM 90m DEM's	ArcGIS format	Generated sun-shaded relief images

Table 1. Statistics of the magnetic susceptibility of different types of igneous rocks in Central Iran.

Rock type	Lithology	Magnetic susceptibility (K, 10^{-3} SI)		Mean of each type
		Range	Mean	
Mafic-ultramafic rock	Ultramafic rocks	25-172	54	48
	Magnetite	42-550	189	
	Peridotite	20-146	76	
	Pyroxenite	20-115	83	
	Gabbro	20-105	37	
	Diabase	30-98	24	
Intermediate-felsic rock	Diorite	7-97	19	14
	Syenite	5-79	41	
	Granite	0-44	5	
	Granodiorite	0-51	6	
Volcanic rock	Basalt	12-178	28	19
	Trachyte	10-270	9	
	Andesite	10-188	21	
	Rhyolite	0-68	12	
	Tuff	0-130	16	

Study Area on Structural Map of Iran

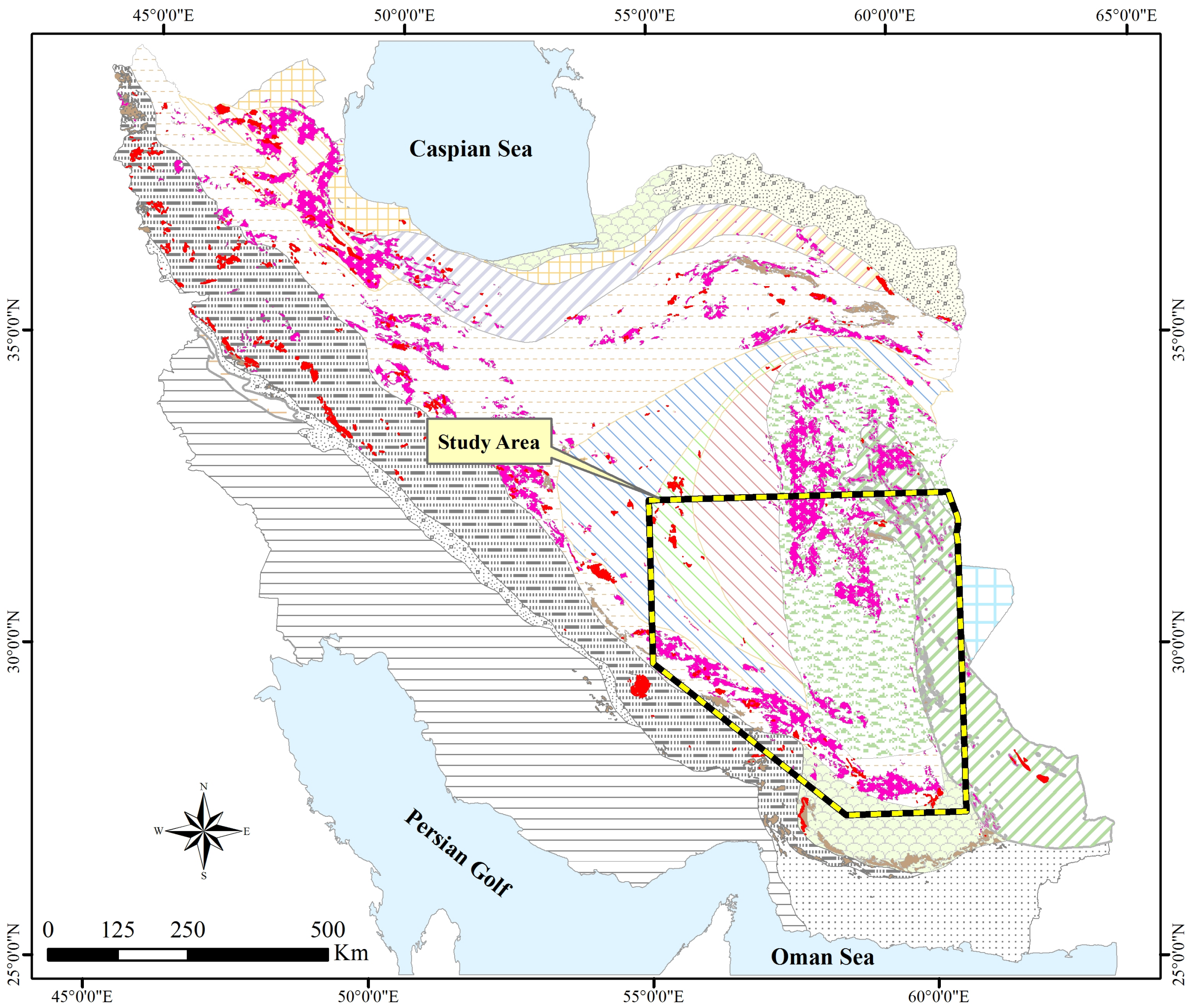

Legend

- Bisetune Structural Subzone
- Central Alborz Geological and Structural Zone
- Central Iran Geological and Structural Zone
- Eastern Alborz Geological and Structural Zone
- Kermanshah Radiolarites Subzone
- Khazar Talesh Ziveh Structural Subzone
- Kopeh Dagh Geological and Structural Zone
- Lut Block
- Makran Accretionary Zone
- Ophiolitic Zone
- Quaternary Depressions
- Zabol Block
- Zagros Structural Zone
- Zone of Metamorphic Rocks and Intruded Granitoides
- Western Alborz Geological and Structural Zone
- Sistan Structural Zone
- Yazd Sub-Zone
- Bafq Posht-e Badam Structural Subzone
- Tabas Structural Subzone
- Intrusive Rocks of Iran
- Tertiary Igneous Rocks
- Sea

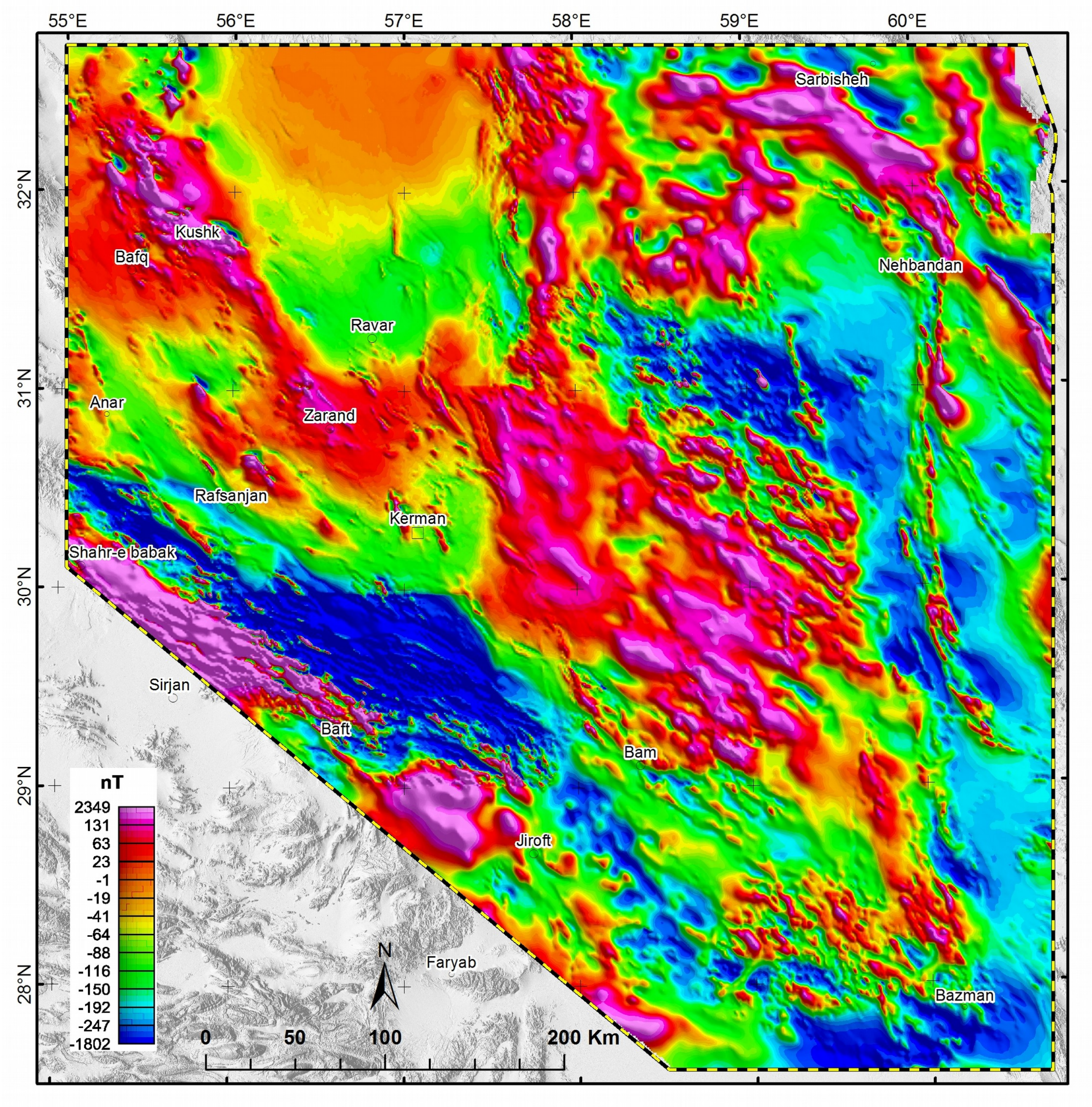

55°E
56°E
57°E
58°E
59°E
60°E
32°N
31°N
30°N
29°N
28°N
Sarbisheh
Kushk
Bafq
Nehbandan
Ravar
Anar
Zarand
Rafsanjan
Kerman
Shahr-e babak
Sirjan
Baft
Bam
Jiroft
Faryab
Bazman
nT
2349
131
63
23
-1
-19
-41
-64
-88
-116
-150
-192
-247
-1802
N
0
50
100
200 Km

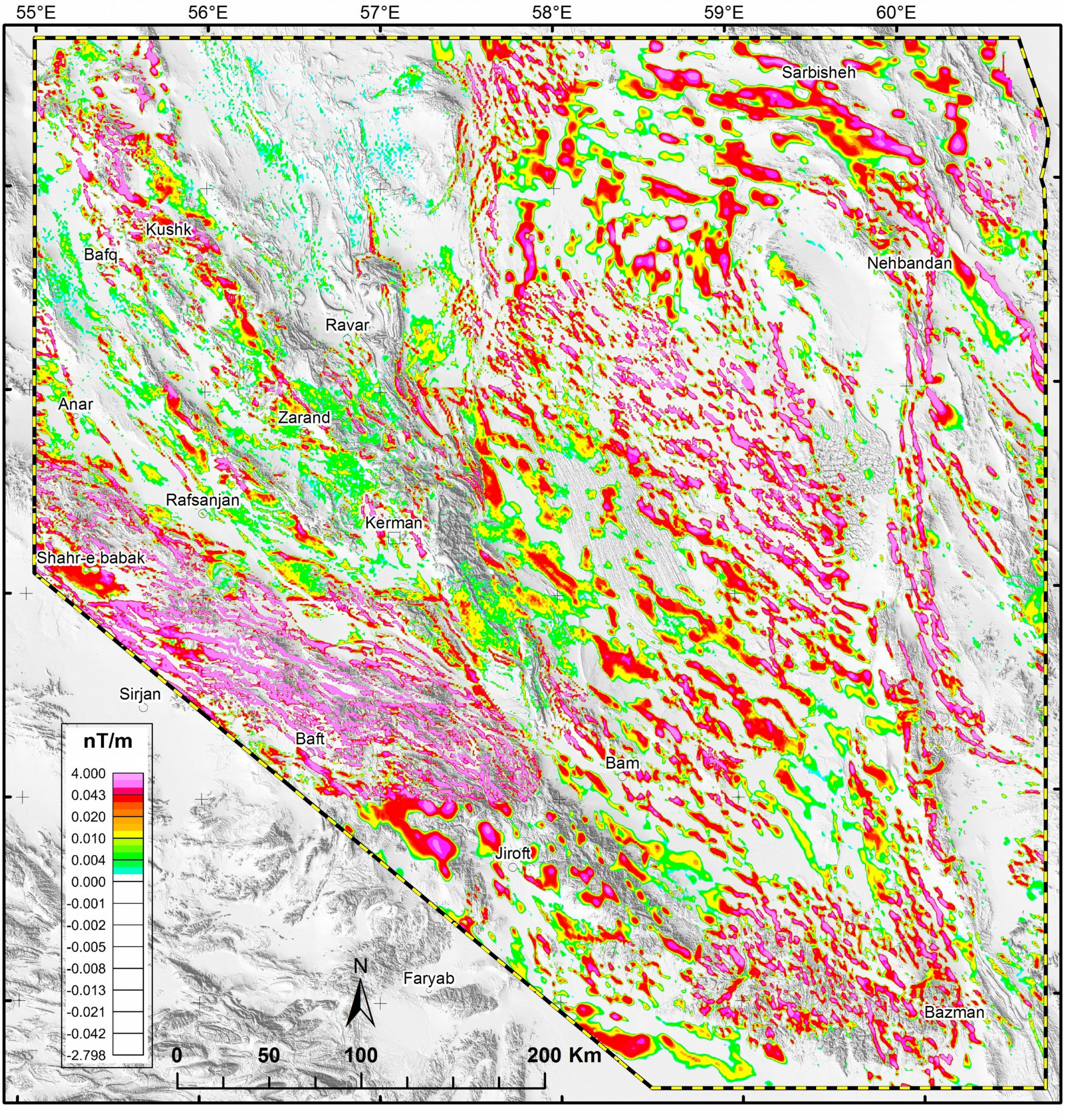

55°E
56°E
57°E
58°E
59°E
60°E
32°N
31°N
30°N
29°N
28°N
Sarbisheh
Kushk
Bafq
Nehbandan
Ravar
Anar
Zarand
Rafsanjan
Kerman
Shahr-e babak
Sirjan
Baft
Bam
Jiroft
Faryab
Bazman
nT/m
4.000
0.043
0.020
0.010
0.004
0.000
-0.001
-0.002
-0.005
-0.008
-0.013
-0.021
-0.042
-2.798
N
0
50
100
200 Km

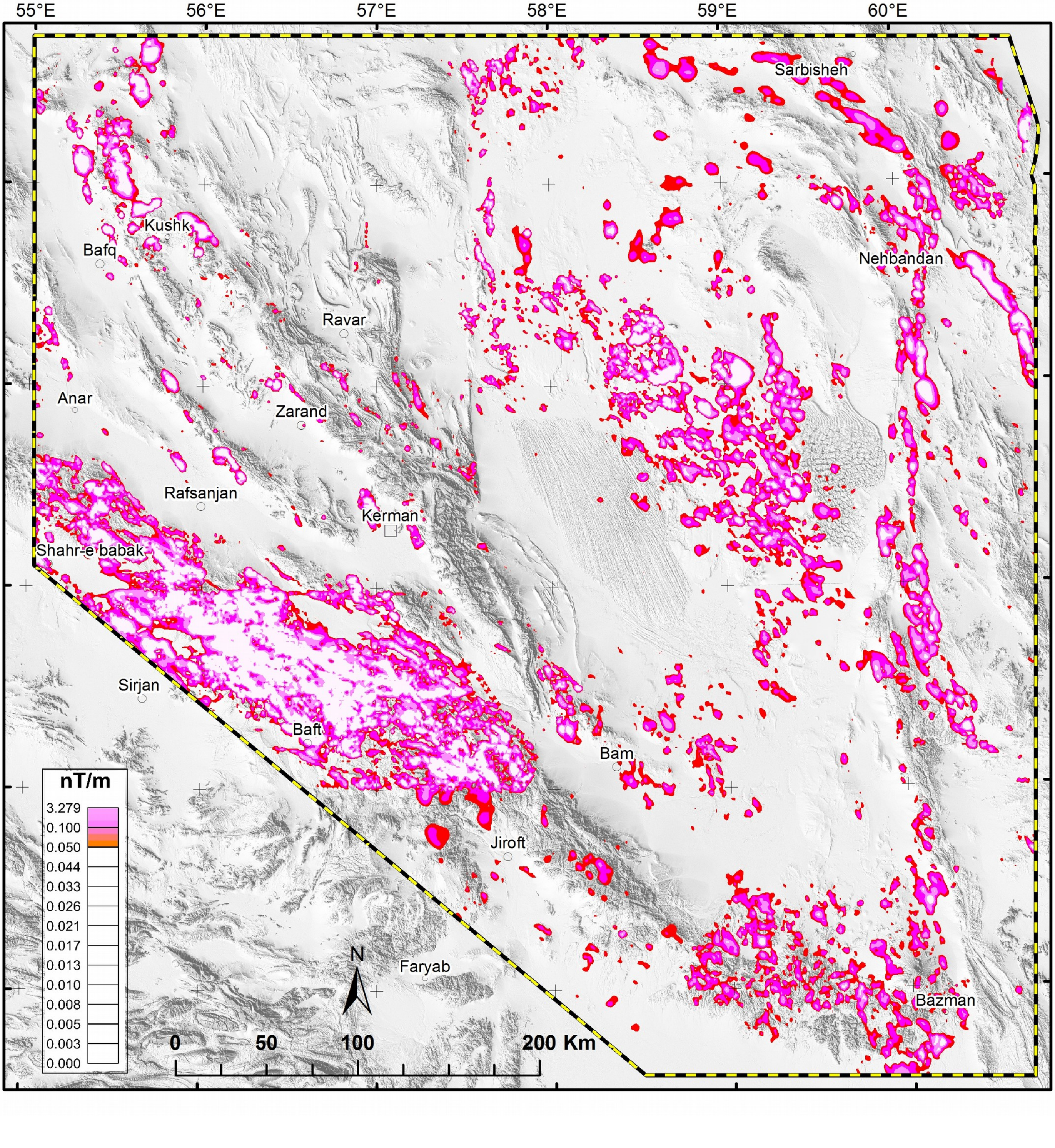

55°E
56°E
57°E
58°E
59°E
60°E
32°N
31°N
30°N
29°N
28°N
Sarbisheh
Kushk
Bafq
Nehbandan
Ravar
Anar
Zarand
Rafsanjan
Kerman
Shahr-e babak
Sirjan
Baft
Bam
Jiroft
Faryab
Bazman
nT/m
3.279
0.100
0.050
0.044
0.033
0.026
0.021
0.017
0.013
0.010
0.008
0.005
0.003
0.000
N
0
50
100
200 Km

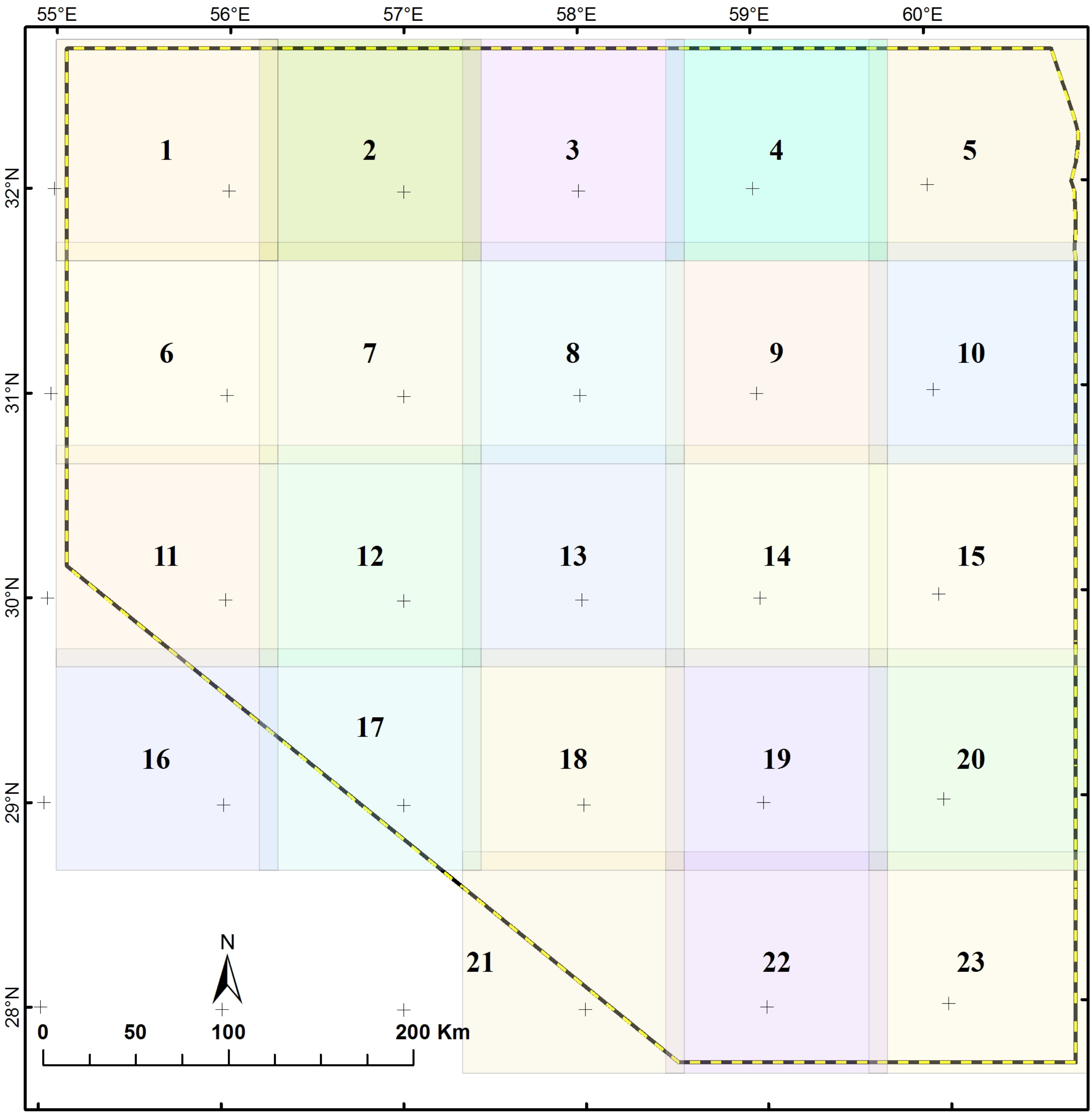
55°E
56°E
57°E
58°E
59°E
60°E
32°N
31°N
30°N
29°N
28°N
1
2
3
4
5
6
7
8
9
10
11
12
13
14
15
16
17
18
19
20
21
22
23
N
0
50
100
200 Km

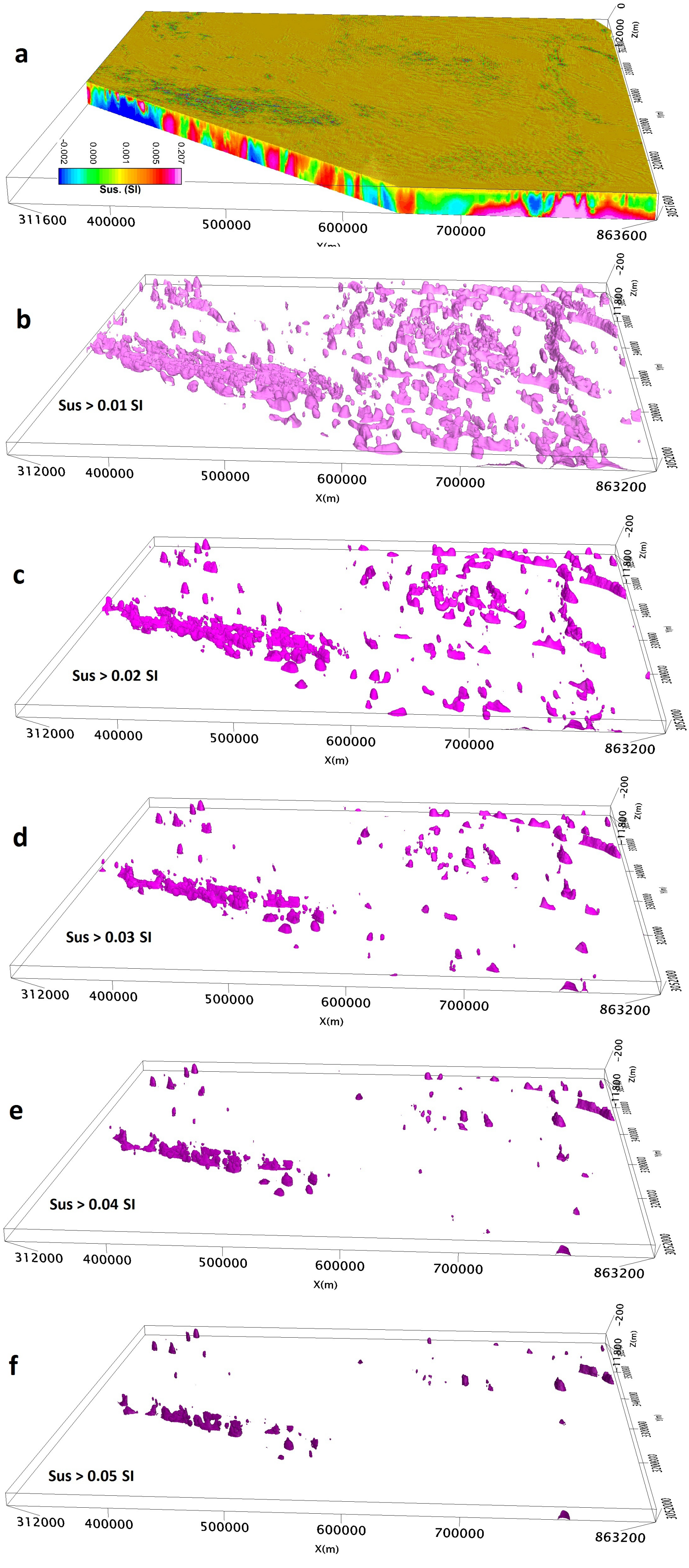
a
Sus. (SI)
-0.002
0.000
0.001
0.005
0.207
311600
400000
500000
600000
700000
863600
Z(m)
0
-12000
b
Sus > 0.01 SI
312000
400000
500000
600000
700000
863200
X(m)
c
Sus > 0.02 SI
d
Sus > 0.03 SI
e
Sus > 0.04 SI
f
Sus > 0.05 SI
-200
-11800

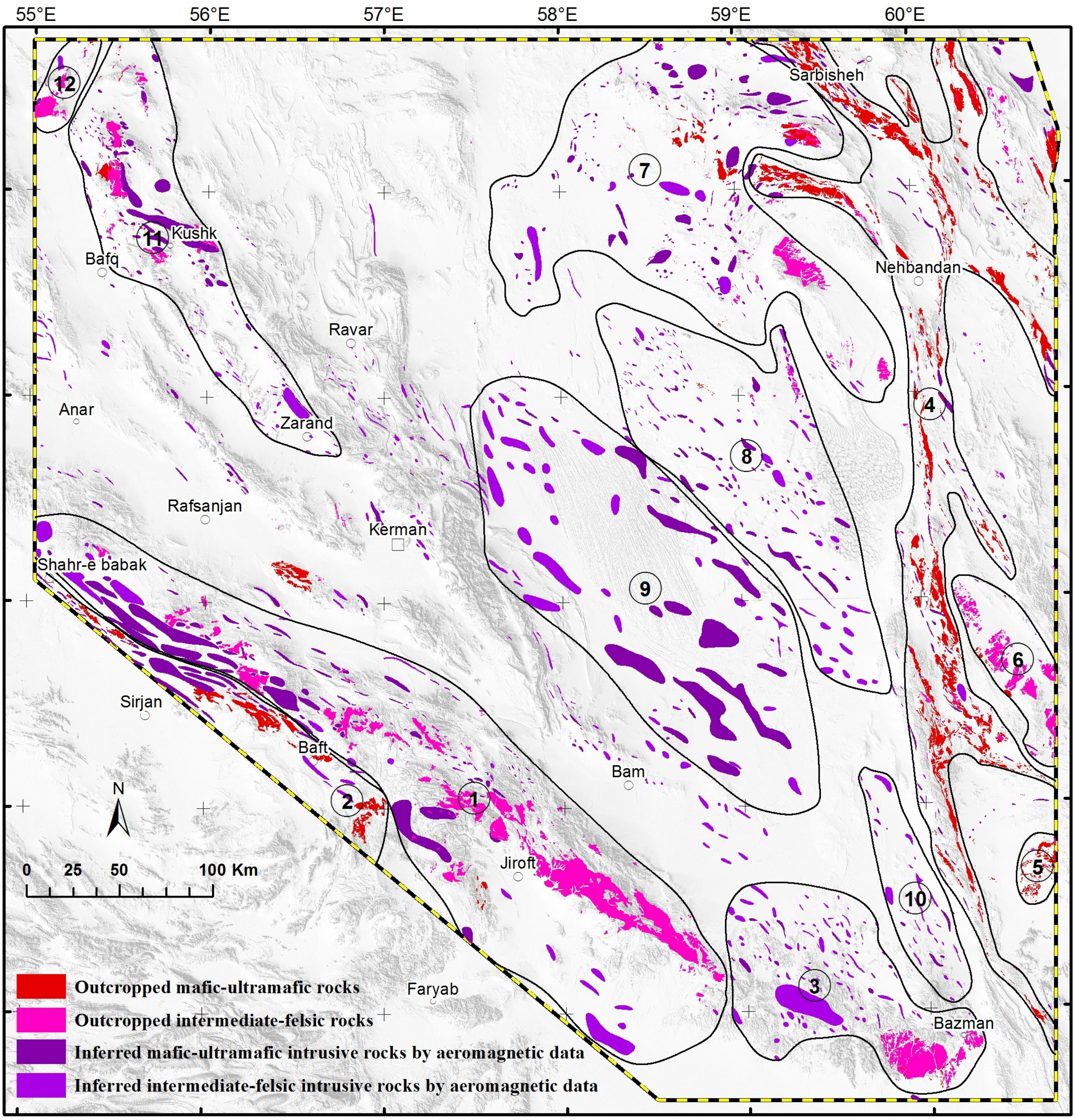

55°E
56°E
57°E
58°E
59°E
60°E
32°N
31°N
30°N
29°N
28°N
Sarbisheh
Nehbandan
Bazman
Kushk
Bafq
Ravar
Anar
Zarand
Rafsanjan
Kerman
Shahr-e babak
Sirjan
Baft
Bam
Jiroft
Faryab
1
2
3
4
5
6
7
8
9
10
11
12
N
0 25 50 100 Km
Outcropped mafic-ultramafic rocks
Outcropped intermediate-felsic rocks
Inferred mafic-ultramafic intrusive rocks by aeromagnetic data
Inferred intermediate-felsic intrusive rocks by aeromagnetic data

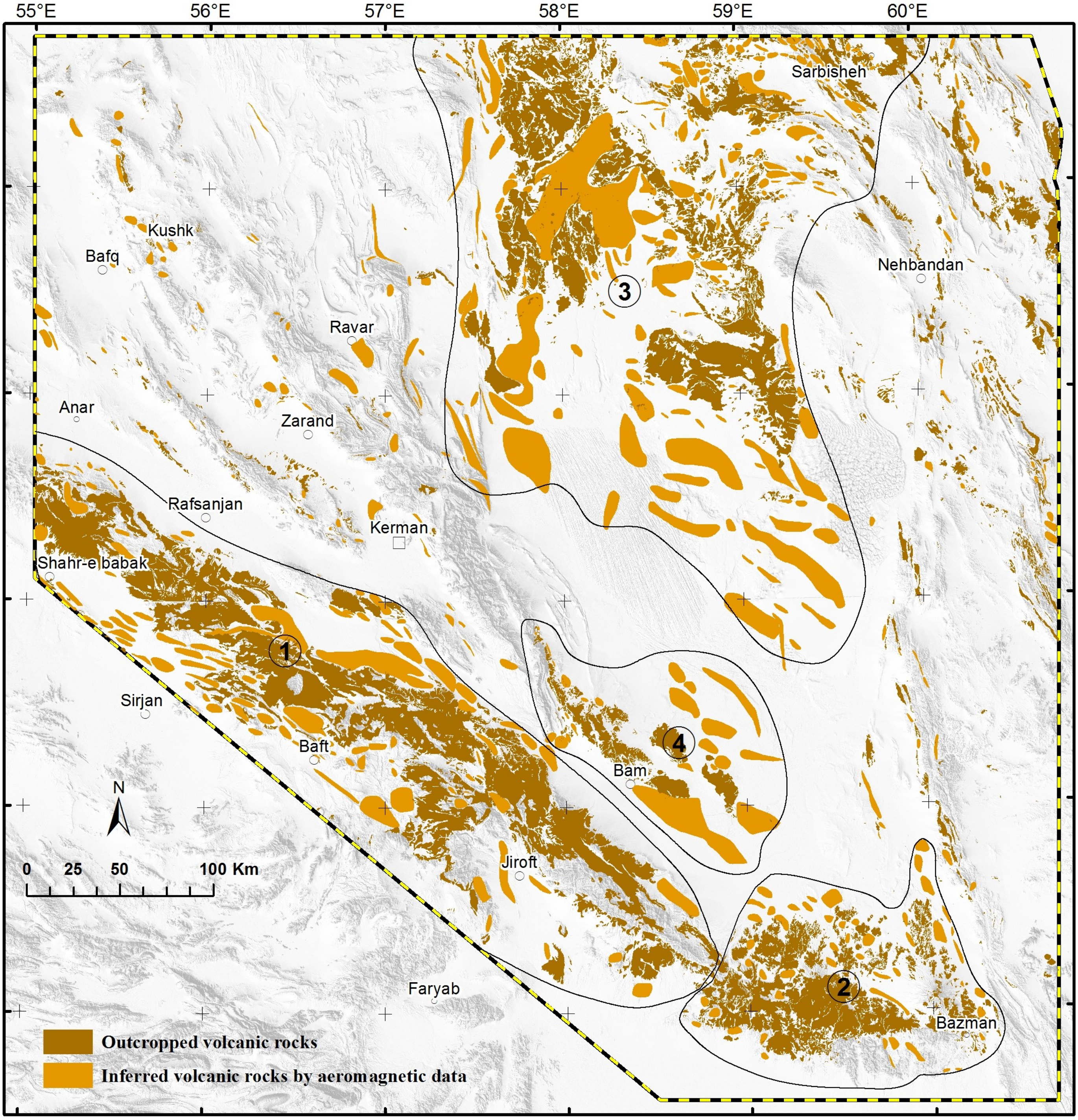

55°E
56°E
57°E
58°E
59°E
60°E
32°N
31°N
30°N
29°N
28°N
Sarbisheh
Kushk
Bafq
Nehbandan
Ravar
Anar
Zarand
Rafsanjan
Kerman
Shahr-e babak
Sirjan
Baft
Bam
Jiroft
Faryab
Bazman
1
2
3
4
N
0 25 50 100 Km
Outcropped volcanic rocks
Inferred volcanic rocks by aeromagnetic data